# Photon Events with Missing Energy in $e^+e^-$ Collisions at $\sqrt{s} = 130$ to 209 GeV

DELPHI Collaboration

## Abstract

The production of single- and multi-photon events has been studied in the reaction $e^+e^- \rightarrow \gamma(\gamma) + invisible\ particles$. The data collected with the DELPHI detector during the years 1999 and 2000 at centre-of-mass energies between 191 GeV and 209 GeV was combined with earlier data to search for phenomena beyond the Standard Model. The measured number of light neutrino families was consistent with three and the absence of an excess of events beyond that predicted by the Standard Model processes was used to set limits on new physics. Both model-independent searches and searches for new processes predicted by supersymmetric and extra-dimensional models have been made. Limits on new non-standard model interactions between neutrinos and electrons were also determined.

J.Abdallah[25], P.Abreu[22], W.Adam[51], P.Adzic[11], T.Albrecht[17], T.Alderweireld[2], R.Alemany-Fernandez[8], T.Allmendinger[17], P.P.Allport[23], U.Amaldi[29], N.Amapane[45], S.Amato[48], E.Anashkin[36], A.Andreazza[28], S.Andringa[22], N.Anjos[22], P.Antilogus[25], W-D.Apel[17], Y.Arnoud[14], S.Ask[26], B.Asman[44], J.E.Augustin[25], A.Augustinus[8], P.Baillon[8], A.Ballestrero[46], P.Bambade[20], R.Barbier[27], D.Bardin[16], G.J.Barker[17], A.Baroncelli[39], M.Battaglia[8], M.Baubillier[25], K-H.Becks[53], M.Begalli[6], A.Behrmann[53], E.Ben-Haim[20], N.Benekos[32], A.Benvenuti[5], C.Berat[14], M.Berggren[25], L.Berntzon[44], D.Bertrand[2], M.Besancon[40], N.Besson[40], D.Bloch[9], M.Blom[31], M.Bluj[52], M.Bonesini[29], M.Boonekamp[40], P.S.L.Booth[23], G.Borisov[21], O.Botner[49], B.Bouquet[20], T.J.V.Bowcock[23], I.Boyko[16], M.Bracko[43], R.Brenner[49], E.Brodet[35], P.Bruckman[18], J.M.Brunet[7], L.Bugge[33], P.Buschmann[53], M.Calvi[29], T.Camporesi[8], V.Canale[38], F.Carena[8], N.Castro[22], F.Cavallo[5], M.Chapkin[42], Ph.Charpentier[8], P.Checchia[36], R.Chierici[8], P.Chliapnikov[42], J.Chudoba[8], S.U.Chung[8], K.Cieslik[18], P.Collins[8], R.Contri[13], G.Cosme[20], F.Cossutti[47], M.J.Costa[50], D.Crennell[37], J.Cuevas[34], J.D'Hondt[2], J.Dalmau[44], T.da Silva[48], W.Da Silva[25], G.Della Ricca[47], A.De Angelis[47], W.De Boer[17], C.De Clercq[2], B.De Lotto[47], N.De Maria[45], A.De Min[36], L.de Paula[48], L.Di Ciaccio[38], A.Di Simone[39], K.Doroba[52], J.Drees[53,8], M.Dris[32], G.Eigen[4], T.Ekelof[49], M.Ellert[49], M.Elsing[8], M.C.Espirito Santo[22], E.Falk[26], G.Fanourakis[11], D.Fassouliotis[11,3], M.Feindt[17], J.Fernandez[41], P.Ferrari[29], A.Ferrer[50], F.Ferro[13], U.Flagmeyer[53], H.Foeth[8], E.Fokitis[32], F.Fulda-Quenzer[20], J.Fuster[50], M.Gandelman[48], C.Garcia[50], Ph.Gavillet[8], E.Gazis[32], R.Gokieli[8,52], B.Golob[43], G.Gomez-Ceballos[41], P.Goncalves[22], E.Graziani[39], G.Grosdidier[20], K.Grzelak[52], J.Guy[37], C.Haag[17], A.Hallgren[49], K.Hamacher[53], K.Hamilton[35], S.Haug[33], F.Hauler[17], V.Hedberg[26], M.Hennecke[17], H.Herr[8], J.Hoffman[52], S-O.Holmgren[44], P.J.Holt[8], M.A.Houlden[23], K.Hultqvist[44], J.N.Jackson[23], G.Jarlskog[26], P.Jarry[40], D.Jeans[35], E.K.Johansson[44], P.D.Johansson[44], P.Jonsson[27], C.Joram[8], L.Jungermann[17], F.Kapusta[25], S.Katsanevas[27], E.Katsoufis[32], G.Kernel[43], B.P.Kersevan[8,43], U.Kerzel[17], A.Kiiskinen[15], B.T.King[23], N.J.Kjaer[8], P.Kluit[31], P.Kokkinias[11], C.Kourkoumelis[3], O.Kouznetsov[16], Z.Krumstein[16], M.Kucharczyk[18], J.Lamsa[1], G.Leder[51], F.Ledroit[14], L.Leinonen[44], R.Leitner[30], J.Lemonne[2], V.Lepeltier[20], T.Lesiak[18], W.Liebig[53], D.Liko[51], A.Lipniacka[44], J.H.Lopes[48], J.M.Lopez[34], D.Loukas[11], P.Lutz[40], L.Lyons[35], J.MacNaughton[51], A.Malek[53], S.Maltezos[32], F.Mandl[51], J.Marco[41], R.Marco[41], B.Marechal[48], M.Margoni[36], J-C.Marin[8], C.Mariotti[8], A.Markou[11], C.Martinez-Rivero[41], J.Masik[12], N.Mastroyiannopoulos[11], F.Matorras[41], C.Matteuzzi[29], F.Mazzucato[36], M.Mazzucato[36], R.Mc Nulty[23], C.Meroni[28], E.Migliore[45], W.Mitaroff[51], U.Mjoernmark[26], T.Moa[44], M.Moch[17], K.Moenig[8,10], R.Monge[13], J.Montenegro[31], D.Moraes[48], S.Moreno[22], P.Morettini[13], U.Mueller[53], K.Muenich[53], M.Mulders[31], L.Mundim[6], W.Murray[37], B.Muryn[19], G.Myatt[35], T.Myklebust[33], M.Nassiakou[11], F.Navarria[5], K.Nawrocki[52], R.Nicolaidou[40], M.Nikolenko[16,9], A.Oblakowska-Mucha[19], V.Obraztsov[42], A.Olshevski[16], A.Onofre[22], R.Orava[15], K.Osterberg[15], A.Ouraou[40], A.Oyanguren[50], M.Paganoni[29], S.Paiano[5], J.P.Palacios[23], H.Palka[18], Th.D.Papadopoulou[32], L.Pape[8], C.Parkes[24], F.Parodi[13], U.Parzefall[8], A.Passeri[39], O.Passon[53], L.Peralta[22], V.Perepelitsa[50], A.Perrotta[5], A.Petrolini[13], J.Piedra[41], L.Pieri[39], F.Pierre[40], M.Pimenta[22], E.Piotto[8], T.Podobnik[43], V.Poireau[8], M.E.Pol[6], G.Polok[18], V.Pozdniakov[16], N.Pukhaeva[2,16], A.Pullia[29], J.Rames[12], A.Read[33], P.Rebecchi[8], J.Rehn[17], D.Reid[31], R.Reinhardt[53], P.Renton[35], F.Richard[20], J.Ridky[12], M.Rivero[41], D.Rodriguez[41], A.Romero[45], P.Ronchese[36], P.Roudeau[20], T.Rovelli[5], V.Ruhlmann-Kleider[40], D.Ryabtchikov[42], A.Sadovsky[16], L.Salmi[15], J.Salt[50], C.Sander[17], A.Savoy-Navarro[25], U.Schwickerath[8], A.Segar[35], R.Sekulin[37], M.Siebel[53], A.Sisakian[16], G.Smadja[27], O.Smirnova[26], A.Sokolov[42], A.Sopczak[21], R.Sosnowski[52], T.Spassov[8], M.Stanitzki[17], A.Stocchi[20], J.Strauss[51], B.Stugu[4], M.Szczekowski[52], M.Szeptycka[52], T.Szumlak[19], T.Tabarelli[29], A.C.Taffard[23], F.Tegenfeldt[49], J.Timmermans[31], L.Tkatchev[16], M.Tobin[23], S.Todorovova[12], B.Tome[22], A.Tonazzo[29], P.Tortosa[50], P.Travnicek[12], D.Treille[8], G.Tristram[7], M.Trochimczuk[52], C.Troncon[28], M-L.Turluer[40], I.A.Tyapkin[16], P.Tyapkin[16], S.Tzamarias[11], V.Uvarov[42], G.Valenti[5], P.Van Dam[31], J.Van Eldik[8], A.Van Lysebetten[2], N.van Remortel[2], I.Van Vulpen[8], G.Vegni[28], F.Veloso[22], W.Venus[37], P.Verdier[27], V.Verzi[38], D.Vilanova[40], L.Vitale[47], V.Vrba[12], H.Wahlen[53], A.J.Washbrook[23], C.Weiser[17], D.Wicke[8], J.Wickens[2],

iii

G.Wilkinson[35], M.Winter[9], M.Witek[18], O.Yushchenko[42], A.Zalewska[18], P.Zalewski[52], D.Zavrtanik[43], V.Zhuravlov[16], N.I.Zimin[16], A.Zintchenko[16], M.Zupan[11]

[1]Department of Physics and Astronomy, Iowa State University, Ames IA 50011-3160, USA
[2]Physics Department, Universiteit Antwerpen, Universiteitsplein 1, B-2610 Antwerpen, Belgium
  and IIHE, ULB-VUB, Pleinlaan 2, B-1050 Brussels, Belgium
  and Faculté des Sciences, Univ. de l'Etat Mons, Av. Maistriau 19, B-7000 Mons, Belgium
[3]Physics Laboratory, University of Athens, Solonos Str. 104, GR-10680 Athens, Greece
[4]Department of Physics, University of Bergen, Allégaten 55, NO-5007 Bergen, Norway
[5]Dipartimento di Fisica, Università di Bologna and INFN, Via Irnerio 46, IT-40126 Bologna, Italy
[6]Centro Brasileiro de Pesquisas Físicas, rua Xavier Sigaud 150, BR-22290 Rio de Janeiro, Brazil
  and Depto. de Física, Pont. Univ. Católica, C.P. 38071 BR-22453 Rio de Janeiro, Brazil
  and Inst. de Física, Univ. Estadual do Rio de Janeiro, rua São Francisco Xavier 524, Rio de Janeiro, Brazil
[7]Collège de France, Lab. de Physique Corpusculaire, IN2P3-CNRS, FR-75231 Paris Cedex 05, France
[8]CERN, CH-1211 Geneva 23, Switzerland
[9]Institut de Recherches Subatomiques, IN2P3 - CNRS/ULP - BP20, FR-67037 Strasbourg Cedex, France
[10]Now at DESY-Zeuthen, Platanenallee 6, D-15735 Zeuthen, Germany
[11]Institute of Nuclear Physics, N.C.S.R. Demokritos, P.O. Box 60228, GR-15310 Athens, Greece
[12]FZU, Inst. of Phys. of the C.A.S. High Energy Physics Division, Na Slovance 2, CZ-180 40, Praha 8, Czech Republic
[13]Dipartimento di Fisica, Università di Genova and INFN, Via Dodecaneso 33, IT-16146 Genova, Italy
[14]Institut des Sciences Nucléaires, IN2P3-CNRS, Université de Grenoble 1, FR-38026 Grenoble Cedex, France
[15]Helsinki Institute of Physics, P.O. Box 64, FIN-00014 University of Helsinki, Finland
[16]Joint Institute for Nuclear Research, Dubna, Head Post Office, P.O. Box 79, RU-101 000 Moscow, Russian Federation
[17]Institut für Experimentelle Kernphysik, Universität Karlsruhe, Postfach 6980, DE-76128 Karlsruhe, Germany
[18]Institute of Nuclear Physics PAN,Ul. Radzikowskiego 152, PL-31142 Krakow, Poland
[19]Faculty of Physics and Nuclear Techniques, University of Mining and Metallurgy, PL-30055 Krakow, Poland
[20]Université de Paris-Sud, Lab. de l'Accélérateur Linéaire, IN2P3-CNRS, Bât. 200, FR-91405 Orsay Cedex, France
[21]School of Physics and Chemistry, University of Lancaster, Lancaster LA1 4YB, UK
[22]LIP, IST, FCUL - Av. Elias Garcia, 14-1$^o$, PT-1000 Lisboa Codex, Portugal
[23]Department of Physics, University of Liverpool, P.O. Box 147, Liverpool L69 3BX, UK
[24]Dept. of Physics and Astronomy, Kelvin Building, University of Glasgow, Glasgow G12 8QQ
[25]LPNHE, IN2P3-CNRS, Univ. Paris VI et VII, Tour 33 (RdC), 4 place Jussieu, FR-75252 Paris Cedex 05, France
[26]Department of Physics, University of Lund, Sölvegatan 14, SE-223 63 Lund, Sweden
[27]Université Claude Bernard de Lyon, IPNL, IN2P3-CNRS, FR-69622 Villeurbanne Cedex, France
[28]Dipartimento di Fisica, Università di Milano and INFN-MILANO, Via Celoria 16, IT-20133 Milan, Italy
[29]Dipartimento di Fisica, Univ. di Milano-Bicocca and INFN-MILANO, Piazza della Scienza 2, IT-20126 Milan, Italy
[30]IPNP of MFF, Charles Univ., Areal MFF, V Holesovickach 2, CZ-180 00, Praha 8, Czech Republic
[31]NIKHEF, Postbus 41882, NL-1009 DB Amsterdam, The Netherlands
[32]National Technical University, Physics Department, Zografou Campus, GR-15773 Athens, Greece
[33]Physics Department, University of Oslo, Blindern, NO-0316 Oslo, Norway
[34]Dpto. Fisica, Univ. Oviedo, Avda. Calvo Sotelo s/n, ES-33007 Oviedo, Spain
[35]Department of Physics, University of Oxford, Keble Road, Oxford OX1 3RH, UK
[36]Dipartimento di Fisica, Università di Padova and INFN, Via Marzolo 8, IT-35131 Padua, Italy
[37]Rutherford Appleton Laboratory, Chilton, Didcot OX11 OQX, UK
[38]Dipartimento di Fisica, Università di Roma II and INFN, Tor Vergata, IT-00173 Rome, Italy
[39]Dipartimento di Fisica, Università di Roma III and INFN, Via della Vasca Navale 84, IT-00146 Rome, Italy
[40]DAPNIA/Service de Physique des Particules, CEA-Saclay, FR-91191 Gif-sur-Yvette Cedex, France
[41]Instituto de Fisica de Cantabria (CSIC-UC), Avda. los Castros s/n, ES-39006 Santander, Spain
[42]Inst. for High Energy Physics, Serpukov P.O. Box 35, Protvino, (Moscow Region), Russian Federation
[43]J. Stefan Institute, Jamova 39, SI-1000 Ljubljana, Slovenia and Laboratory for Astroparticle Physics,
  Nova Gorica Polytechnic, Kostanjeviska 16a, SI-5000 Nova Gorica, Slovenia,
  and Department of Physics, University of Ljubljana, SI-1000 Ljubljana, Slovenia
[44]Fysikum, Stockholm University, Box 6730, SE-113 85 Stockholm, Sweden
[45]Dipartimento di Fisica Sperimentale, Università di Torino and INFN, Via P. Giuria 1, IT-10125 Turin, Italy
[46]INFN,Sezione di Torino, and Dipartimento di Fisica Teorica, Università di Torino, Via P. Giuria 1,
  IT-10125 Turin, Italy
[47]Dipartimento di Fisica, Università di Trieste and INFN, Via A. Valerio 2, IT-34127 Trieste, Italy
  and Istituto di Fisica, Università di Udine, IT-33100 Udine, Italy
[48]Univ. Federal do Rio de Janeiro, C.P. 68528 Cidade Univ., Ilha do Fundão BR-21945-970 Rio de Janeiro, Brazil
[49]Department of Radiation Sciences, University of Uppsala, P.O. Box 535, SE-751 21 Uppsala, Sweden
[50]IFIC, Valencia-CSIC, and D.F.A.M.N., U. de Valencia, Avda. Dr. Moliner 50, ES-46100 Burjassot (Valencia), Spain
[51]Institut für Hochenergiephysik, Österr. Akad. d. Wissensch., Nikolsdorfergasse 18, AT-1050 Vienna, Austria
[52]Inst. Nuclear Studies and University of Warsaw, Ul. Hoza 69, PL-00681 Warsaw, Poland
[53]Fachbereich Physik, University of Wuppertal, Postfach 100 127, DE-42097 Wuppertal, Germany

# 1   Introduction

The DELPHI experiment has previously reported studies of events at centre-of-mass energies up to 189.2 GeV in which only one photon or two acoplanar[1] photons were produced [1–5]. The other LEP experiments have reported similar studies [6]. The present paper combines all DELPHI single-photon data recorded at 180-209 GeV and all acoplanar two-photon data recorded at 130-209 GeV to obtain the most stringent limits on new physics. The paper improves and supersedes the earlier studies made at lower energies.

At LEP2, the Standard Model predicts that events with one or more photons and invisible particles are produced mainly by the reaction $e^+e^- \to \nu\bar{\nu}\gamma(\gamma)$ which receives a contribution from Z-exchange in the $s$-channel with single- or multi-photon emission from the initial state electrons and from the $t$-channel $W$-exchange, with the photon(s) radiated from the beam electrons or the exchanged $W$. Beyond the Standard Model, contributions to the $\gamma + missing\ energy$ final state could come from a new generation of neutrinos or from the production of some new particle, stable or unstable, weakly interacting or decaying into a photon and an invisible particle.

A measurement of the cross-section of the process $e^+e^- \to \nu\bar{\nu}\gamma$ determines the number of light neutrino generations, $N_\nu$. DELPHI has previously reported measurements of $N_\nu$ using both LEP1 [1] and LEP2 [5] single-photon data and this measurement has now been re-evaluated with all 180-209 GeV DELPHI data.

The $e^+e^- \to \nu\bar{\nu}\gamma$ cross-section can also be used to calculate limits on new neutrino interactions with electrons, beyond what is predicted by the Standard Model. A set of limits on the parameter space for such new neutral-current interactions is presented in this paper.

A search for new particles can be done both in the framework of specific models and in a model-independent way. The event topology with one or two photons and missing energy can be used to look for the production of either new invisible particles tagged by initial-state radiation (ISR) or the production of invisible particles in association with a photon. The model-independent single-photon searches described in this paper take both of these possibilities into account. The first search is for the production of a new hypothetical particle tagged by an ISR-photon, $e^+e^- \to X\gamma$. In this analysis, the new particle, $X$, was assumed to be either stable and weakly interacting or to be decaying into invisible decay products. The second model-independent search consisted of looking for and setting cross-section limits on the process $e^+e^- \to XY \to YY\gamma$ where $X$ is a hypothetical new neutral particle which decays radiatively to $Y$ which is a stable weakly interacting new neutral particle.

A specific case in which photons are produced in association with a new particle was addressed in the search for gravitons via the process $e^+e^- \to \gamma G$. The existence of this process has been predicted by some string models [7,8] in which gravity is allowed to propagate in a space with more dimensions than the usual four space-time dimensions.

Various theories of supersymmetry (SUSY) predict the existence of new particles which would produce final states with missing energy and one or several photons. Different assumptions about the SUSY breaking mechanism lead to two main search scenarios in which the Lightest Supersymmetric Particle (LSP) is either the gravitino ($\tilde{G}$) or the neutralino ($\tilde{\chi}_1^0$).

Gauge-Mediated Supersymmetry Breaking (GMSB) models [9] typically predict that the gravitino is the LSP with a mass less than a few hundred eV/c$^2$ and that the neutralino

---
[1]The acoplanarity is here defined as $180° - \Phi_{12}^T$, where $\Phi_{12}^T$ is the angle between the two photons in the plane perpendicular to the beam axis.

or the slepton is the Next-to-Lightest Supersymmetric Particle (NLSP). If the neutralino is the NLSP it decays into $\tilde{G}\gamma$ with the gravitino being essentially massless and undetectable and it is possible to search for both single-photon and multi-photon production via the processes $e^+e^- \to \tilde{G}\tilde{\chi}_1^0 \to \tilde{G}\tilde{G}\gamma$ and $e^+e^- \to \tilde{\chi}_1^0\tilde{\chi}_1^0 \to \tilde{G}\gamma\tilde{G}\gamma$. The cross-section for the single-photon process is proportional to $1/m_{\tilde{G}}^2$ while the two-photon process does not depend on the gravitino mass. Therefore the search for $e^+e^- \to \tilde{G}\tilde{\chi}_1^0 \to \tilde{G}\tilde{G}\gamma$ at LEP is only sensitive if the gravitino is ultralight ($m_{\tilde{G}} < 10^{-4}$ eV/c$^2$).

If the gravitino is the LSP and it is the only supersymmetric particle which is kinematically accessible, it is possible to search for $e^+e^- \to \tilde{G}\tilde{G}\gamma$ [10] by using ISR-photons to tag the undetectable production of a gravitino pair. This search makes it possible to set a lower limit on the gravitino mass ($m_{\tilde{G}}$) and the DELPHI collaboration is in this paper updating the calculation of this limit using all available data with $\sqrt{s} >$180 GeV.

The NLSP lifetime depends on the gravitino mass and if this is sufficiently large (a few hundred eV/c$^2$) the neutralinos in $e^+e^- \to \tilde{\chi}_1^0\tilde{\chi}_1^0 \to \tilde{G}\gamma\tilde{G}\gamma$ will decay in such a way that the detected photons will not originate at the beam interaction point. When the mean decay paths are comparable to the detector scale, events with a single photon not pointing to the interaction region are expected and has been searched for.

In gravity-mediated SUSY breaking (SUGRA) models [11], the gravitino is typically heavy with a mass of several hundreds of GeV/c$^2$ and it is the neutralinos which are the LSP and NLSP. Under certain assumptions, $\tilde{\chi}_2^0$ will decay into a stable undetectable $\tilde{\chi}_1^0$ and a photon. This can give rise to processes such as $e^+e^- \to \tilde{\chi}_1^0\tilde{\chi}_2^0 \to \tilde{\chi}_1^0\tilde{\chi}_1^0\gamma$ and $e^+e^- \to \tilde{\chi}_2^0\tilde{\chi}_2^0 \to \tilde{\chi}_1^0\gamma\tilde{\chi}_1^0\gamma$ with both single- and two-photon production. A search for the two-photon process has been carried out but since the predicted cross-section for the single-photon process is small the previously mentioned model-independent search for $e^+e^- \to XY \to YY\gamma$ will be presented instead.

There exists in addition a so-called "no-scale" supergravity model (also known as the LNZ model) [12] in which the local supersymmetry breaking is decoupled from the global supersymmetry breaking. This results in the prediction of an ultralight gravitino and the process $e^+e^- \to \tilde{G}\tilde{\chi}_1^0 \to \tilde{G}\tilde{G}\gamma$. The main phenomenological difference between this model and the GMSB model is that only the gravitino and neutralino masses are free parameters since the selectron masses and the neutralino composition depend on the neutralino mass in the no-scale supergravity model.

This paper describes the single- and multi-photon selection criteria, the measurement of the single-photon cross-section and the number of neutrino families and it gives limits on non-Standard Model physics obtained from searches for gravitons in extra-dimensional models and supersymmetric particles.

# 2   The DELPHI detector

The general criteria for the selection of events are based mainly on the electromagnetic calorimeters and the tracking system of the DELPHI detector [13]. All three major electromagnetic calorimeters in DELPHI, the High density Projection Chamber (HPC), the Forward ElectroMagnetic Calorimeter (FEMC) and the Small angle TIle Calorimeter (STIC), have been used in the single-photon reconstruction while only the FEMC and the HPC were used in the multi-photon analysis. For the study of the non-pointing single-photon events only the HPC detector was used.

The barrel region of DELPHI was covered by the HPC, which was a gas sampling calorimeter able to sample a shower nine times longitudinally. The FEMC was made up of an array of 4532 lead glass blocks in each endcap. The energy resolution of this

calorimeter was degraded by the material in front of it, which caused photon conversions and even preshowers. The very forward luminosity monitor STIC [14] consisted of two cylindrical lead-scintillator calorimeters read out by wavelength-shifting fibres. Two layers of scintillators mounted on the front of each STIC calorimeter together with a smaller ring-shaped scintillator mounted directly on the beampipe, provided $e-\gamma$ separation. The angular coverages of these calorimeters and the energy resolutions[2] are given in Table 1 and the detailed characteristics and performances are described in [13,14].

Three different triggers were used in DELPHI to select single-photon events. The HPC trigger for purely neutral final states used a plane of scintillators inserted into one of the HPC sampling gaps at a depth of around 4.5 radiation lengths. A second level trigger decision was produced from the signals of analog electronics and was based on a coincidence pattern inside the HPC module. The trigger efficiency has been measured with Compton and Bhabha events. It was strongly dependent on the photon energy, $E_\gamma$, rising steeply up to $\sim$10 GeV, with about 52% efficiency at 6 GeV and above 77% when $E_\gamma > 30$ GeV. It reached a maximum of 84% at $E_\gamma \simeq E_{\rm beam}$. The FEMC trigger required an energy deposition of at least 2.5 GeV. The efficiency increased with energy and was 93% at 10 GeV and above 99% for $E_\gamma > 15$ GeV. Correlated noise in several adjacent channels caused fake triggers, but these could be rejected offline with high efficiency by algorithms that took into account the lead glass shower pattern. The STIC trigger required an energy deposition of at least 15 GeV and it was furthermore required that there was no signal in at least one of the two scintillator planes in front of the shower. The energy requirement caused inefficiencies for showers with less than 30 GeV of energy. The efficiency of the scintillator requirement has been measured with samples of photons from $e^+e^-\gamma$ and $q\bar{q}\gamma$ events. The efficiency varied between 70% and 33% over the angular region used in the analysis.

In addition to the electromagnetic calorimeters, the DELPHI tracking system was used to reject events in which charged particles were produced. The main tracking devices were the Time Projection Chamber (TPC) and the silicon microVertex Detector (VD) and its extension into the forward region, the Very Forward Tracker (VFT). The silicon trackers were also used for electron/photon separation by vetoing photon candidates which could be associated with hits in these detectors.

Finally, the Hadron CALorimeter (HCAL) and its cathode-read-out system were used to reject cosmic rays and to provide photon/hadron separation, while the DELPHI Hermeticity Taggers were used to ensure complete detector hermeticity for additional neutral particles.

| | Type | Angular coverage | $\sigma_E/E$ | $X_0$ |
|---|---|---|---|---|
| STIC: | Lead/scint. | $2° < \theta < 10°$ , $170° < \theta < 178°$ | $0.0152 \oplus (0.135/\sqrt{E})$ | 27 |
| FEMC: | Lead glass | $10° < \theta < 37°$ , $143° < \theta < 170°$ | $0.03 \oplus (0.12/\sqrt{E}) \oplus (0.11/E)$ | 20 |
| HPC: | Lead/gas | $40° < \theta < 140°$ | $0.043 \oplus (0.32/\sqrt{E})$ | 18 |

Table 1: Polar angle coverage, energy resolution (where $E$ is in GeV and $\oplus$ denotes addition in quadrature) and thickness (in radiation lengths) of the electromagnetic calorimeters in DELPHI.

---

[2] The FEMC energy resolution in Table 1 was measured with electrons that had not interacted before reaching the calorimeter and if preshowering electrons are taken into account the constant term has to be increased to 0.057 .

# 3 Event selection

## 3.1 Single-photon events

The single-photon events were selected in two stages. In the first stage, events with only one detected photon were preselected and compared to the Standard Model process $e^+e^- \to \nu\bar{\nu}\gamma$. These events were also used to calculate cross-sections and for a determination of the number of light neutrino families. A likelihood ratio method was then used to maximize the sensitivity in the various single-photon searches.

### 3.1.1 Preselection

Different analyses were made depending on the electromagnetic calorimeter in which the photon candidate was found:

- Events with a photon in the HPC were selected by requiring a shower having a scaled energy $x_\gamma = E_\gamma/E_{beam} > 0.06$ and a polar angle, $\theta$, between $45°$ and $135°$ and no charged particle tracks. Electronic noise and alpha particles emitted from the lead converter created fake low-energy showers in the HPC but these could be rejected very effectively by requiring the longitudinal shower profile to satisfy conditions defining a good electromagnetic shape [2]. Backgrounds from radiative Bhabha events and Compton events were rejected by requiring no other electromagnetic showers in the event unless they were in the HPC and within $20°$ of the first one. Cosmic rays were rejected mainly by the hadron calorimeter. If there were two or more hadronic showers the event was discarded and if only one HCAL shower was present, the event was rejected if the shower was not consistent with being caused by punch-through of the electromagnetic shower. The requirement of no charged particles also removed cosmic ray background. In addition, a constraint on the $\gamma$ direction was imposed, requiring that the line of flight from the mean interaction point and the shower direction measured in the calorimeter coincided within $15°$.
  The offline photon identification and reconstruction efficiency was determined on the basis of a Monte Carlo sample of events passed through the complete simulation of the DELPHI detector [13]. The efficiency depended on the photon energy and it ranged from 41% at 6 GeV to 78% for $E_\gamma > 80$ GeV. In addition, some efficiencies were determined from data. In particular, the requirements of no electromagnetic or hadronic showers and no charged particles were studied. A sample of events triggered at random and a sample of back-to-back Bhabha events with the electrons in the STIC were used for this purpose. It was found that noise and machine background caused showers and tracks which would veto about 7% of the good single-photon events and the data was corrected for this loss.
- Events with at least one shower in the FEMC with a scaled energy $x_\gamma > 0.10$ and a polar angle in the intervals $12° < \theta < 32°$ or $148° < \theta < 168°$ were selected. The large background of radiative Bhabha events made it necessary to add an energy-dependent angular requirement, $\theta > 28° - 80° \cdot x_\gamma$ (and the complementary $\theta$-region). This cut only affected the very low energy region $x_\gamma < 0.20$. In order to separate electrons from photons, the event was rejected if hits in the silicon microvertex detectors (VD and VFT) could be associated with the FEMC shower. The showers in the inner ($10° < \theta < 12°$) and outer ($32° < \theta < 37°$) radial parts of the FEMC were discarded because of the large amount of material (about $2X_0$) in front of the FEMC due to the STIC and the TPC detectors. The material in front of the FEMC

meant that about half of the photons preshowered before reaching the calorimeter. Most of the preshower was contained in a cone of about 15° around the largest shower and the selection took this into account by requiring no charged particle tracks, no other electromagnetic showers and no hadronic showers outside a 15° cone. If there were no charged particle tracks inside the cone either, i.e., the photon had not preshowered, it was required that only one FEMC shower was present in the event. If, on the other hand, charged particle tracks were present in the cone, more FEMC showers were allowed and their momentum vectors were added to that of the largest shower. The requirement of no electromagnetic showers outside the cone greatly reduced the background of radiative Bhabha and Compton events by rejecting events that had one or both electrons in the acceptance of the experiment. Events due to cosmic rays were rejected by the requirement of no hadronic showers outside the cone. Inside the cone, hadronic energy was allowed only in the first layer of the HCAL.

Most reconstruction and event selection efficiencies in the analysis were taken into account by using Monte Carlo samples passed through the extensive detector simulation package of DELPHI [13]. These efficiencies were estimated to be between 57% and 75% . The additional loss of events due to noise and machine background was estimated by using Bhabha events and random triggered data samples. The calculation showed that about 11% of the single-photon events in FEMC were lost.

- Single photons in the STIC were preselected by requiring one shower with a scaled energy $x_\gamma > 0.30$ and with $3.8° < \theta < 8°$ or $172° < \theta < 176.2°$. The large background coming from beam-gas interactions made it necessary to add an energy-dependent angular requirement, $\theta > 9.2° - 9° \cdot x_\gamma$ (and the complementary $\theta$-region). This cut only affected the energy region $x_\gamma < 0.60$ . It was furthermore required that there were no other electromagnetic showers, no hadronic showers and no charged particles in the event. All single-photon candidates had to satisfy the STIC single-photon trigger. A requirement of no signal in the small scintillators mounted on the beampipe made it possible to reject radiative $ee\gamma$ background.

  The losses of photons in STIC, due to the offline photon identification and reconstruction, were estimated to be 5% in an analysis using $e^+e^-\gamma$ and $q\bar{q}\gamma$ events. The selection of events with no additional shower in the STIC and no tracks implied similar losses (7%) to those found in the HPC analysis and were estimated with the same methods.

The result of the single-photon event selection described above was that events with more than one photon could survive if the other photons were at low angle ($\theta_\gamma < 2.2°$), low energy ($E_\gamma < 0.8$ GeV) or within 3°, 15° and 20° from the highest energy photon in the STIC, FEMC and HPC respectively.

### 3.1.2 Final selection

A likelihood ratio method was used to select the final sample of events in the various searches using single-photon events. The photon energy was used as the final discriminating variable and two likelihood functions ($f_S(E_\gamma)$ and $f_B(E_\gamma)$) were produced from the normalized photon energy distributions of the simulated signal and background events, after passing through the same selection criteria. The likelihood ratio function was defined as $\mathcal{L}_R = f_S(E_\gamma)/f_B(E_\gamma)$ where an event with $\mathcal{L}_R > \mathcal{L}_R^{CUT}$ was selected as a candidate event. The value of $\mathcal{L}_R^{CUT}$ was optimised to give the minimum signal cross-section ex-

cluded at 95% C.L. in the absence of a signal:

$$\sigma^{min}(\mathcal{L}_R^{CUT}) = \frac{N_{95}^{min}(\mathcal{L}_R^{CUT})}{\epsilon^{max}(\mathcal{L}_R^{CUT}) \times L}$$

where $N_{95}^{min}$ is the upper limit on the number of signal events at 95% C.L., $\epsilon^{max}$ is the efficiency for the signal and L is the integrated luminosity. This method optimises the background suppression for a given signal efficiency [15]. A more detailed description of the method can be found in [16].

The data collected at different centre-of-mass energies were analysed separately and different analyses were made depending on the electromagnetic calorimeter in which the photon was recorded. The final experimental limits were obtained using a Bayesian multi-channel method [16] which combined the results from up to 20 analyses. The method takes into account all the available information (such as the fraction of the signal and the average background in each subdetector and in each data subsample), and this makes it possible to calculate optimum limits.

## 3.2 Multi-photon events

Multi-photon events were selected by a two-step procedure. In the first preselection step, events with at least two photons and missing energy were selected. This sample was dominated by the Standard Model process $e^+e^- \rightarrow \nu\bar{\nu}\gamma\gamma(\gamma)$ and it was used to monitor the modelling of this process by the KORALZ 4.02 generator [17]. In a second step, the selection criteria were tightened in order to improve the experimental sensitivity to possible signals of supersymmetry, such as the $e^+e^- \rightarrow \tilde{\chi}_1^0\tilde{\chi}_1^0 \rightarrow \tilde{G}\gamma\tilde{G}\gamma$ or $e^+e^- \rightarrow \tilde{\chi}_2^0\tilde{\chi}_2^0 \rightarrow \tilde{\chi}_1^0\gamma\tilde{\chi}_1^0\gamma$ processes. This was achieved by imposing more stringent requirements on the photon polar angles as well as on the event missing mass and transverse momentum.

### 3.2.1 Preselection

The preselection required that there were at least two electromagnetic clusters in the HPC and FEMC detectors with $x_\gamma > 0.05$ and that the event had a total visible energy $E_{vis} < 0.9\sqrt{s}$ and a total transverse momentum $p_T > 0.03E_{miss}$ where $E_{miss} = \sqrt{s} - E_{vis}$. The polar angles of the clusters were required to be in the region $10° < \theta < 170°$ with at least one cluster in $25° < \theta < 155°$. The clusters were identified as photons by requiring that there were no reconstructed charged particle tracks and no hits in the VD or VFT detectors that could be associated with the clusters.

All FEMC and HPC showers in a cone of $10°$ around the shower with the highest energy were merged together. Noise and clusters from alpha particles in the HPC were rejected by requirements on the longitudinal shower profile [4] and the reconstructed HPC shower axis had to point to the interaction point within $25°$.

In order to reduce the background from $e^+e^- \rightarrow \gamma\gamma$ events it was required that the acoplanarity was greater than $3°$. A requirement of no hits in the Hermeticity Taggers reduced the background of $e^+e^- \rightarrow \gamma\gamma\gamma$ where one photon was lost in the holes between the calorimeters. By requiring that the acoplanarity was less than $140°$ when $|\theta_{\gamma1} - \theta_{\gamma2}| < 20°$ it was possible to eliminate single-photon events with the photon converting in the material in front of the calorimeters and producing two separate clusters. Cosmic ray events were rejected by vetoing on energy deposits in the external layers of the HCAL. Doubly radiative Bhabha events where the electrons escape detection along the beampipe could be rejected by requiring that the energy in the STIC was less than $0.02\sqrt{s}$ and that the polar angle of the missing momentum was in the region $10° < \theta_{miss} < 170°$.

If an event had three electromagnetic clusters passing the previous selection it was retained if it had $E_{vis} < 0.8\sqrt{s}$ and the sum of the angles between the three observed photons was less than 358°, i.e., if the event was significantly aplanar. Events with four or more electromagnetic clusters were discarded.

### 3.2.2  Final selections

The final selection in the search for $e^+e^- \to \tilde{\chi}_1^0\tilde{\chi}_1^0 \to \tilde{G}\gamma\tilde{G}\gamma$ required that the scaled transverse momentum for each cluster satisfied $p_{T\gamma}/E_{beam} > 0.07$ if the missing mass ($M_{miss}$) was larger than 60 GeV/c$^2$. This requirement strongly suppressed the Standard Model background coming from $e^+e^- \to \nu\bar{\nu}\gamma\gamma(\gamma)$ where the photons, being emitted from the initial state particles, have a relatively low transverse momentum. A more stringent requirement of $p_{T\gamma}/E_{beam} > 0.14$ was used when the missing mass was close to the Z mass ($80 < M_{miss} < 110$ GeV/c$^2$) and the background was larger. It was in addition required that the energies and angles of the detected photons were compatible with those expected for a particular $\tilde{\chi}_1^0$ mass.

In the search for $e^+e^- \to \tilde{\chi}_2^0\tilde{\chi}_2^0 \to \tilde{\chi}_1^0\gamma\tilde{\chi}_1^0\gamma$, the cut on transverse momentum was replaced by a cut on the polar angle of the photons. It was required that $20° < \theta_\gamma < 160°$ for $M_{miss} > 60$ GeV/c$^2$ with the exception of the Z-region ($80 < M_{miss} < 110$ GeV/c$^2$) where the polar angle was required to fulfil $40° < \theta_\gamma < 140°$. The energies of the detected photons had to be compatible with those expected for a particular pair of $\tilde{\chi}_1^0$ and $\tilde{\chi}_2^0$ masses.

The efficiency of the selection was studied using simulated $e^+e^- \to \tilde{\chi}_1^0\tilde{\chi}_1^0 \to \tilde{G}\gamma\tilde{G}\gamma$ and $e^+e^- \to \tilde{\chi}_2^0\tilde{\chi}_2^0 \to \tilde{\chi}_1^0\gamma\tilde{\chi}_1^0\gamma$ events. The estimated efficiency was in the range 40-55% for both search scenarios [4].

## 3.3  Non-pointing single-photon events

The fine granularity of the HPC calorimeter provided a precise reconstruction of the axis direction in electromagnetic showers. This feature was used to select events with a single photon whose flight direction did not point to the beam interaction region. Events with a single non-pointing photon are expected when two neutral particles with large mean decay paths ($> 4$ m) are produced which subsequently decay into a photon and an invisible particle since the probability that both photons are recorded is then small.

Events of this kind were searched for by requiring one photon in the HPC calorimeter with $E_\gamma > 10$ GeV and an impact parameter exceeding 40 cm. A more stringent HPC cluster selection was made compared to the multi-photon selection [4]. This was done in order to reject noise and cosmic ray events which were a larger problem in the non-pointing single-photon analysis.

It was required that the events had no reconstructed tracks and that no hits in the vertex detector could be found along a line going from the interaction point to the electromagnetic shower. Cosmic ray events, which represented the main background, were largely reduced by vetoing on isolated hits or tracks in the Hermeticity Taggers and signals from the external HCAL layers and from the cathode-read-out system of the hadron calorimeter.

The efficiency of the selection was studied using simulated $e^+e^- \to \tilde{\chi}_1^0\tilde{\chi}_1^0 \to \tilde{G}\gamma\tilde{G}\gamma$ events that had passed through the entire DELPHI detector simulation package. For a mean decay path of 3-8 m the probability that a neutralino would decay before the HPC was small and the total efficiency (including acceptance) was only 4-5% [4].

# 4 Real data and simulated samples

## 4.1 Data samples

The ten data samples that were used in the single-photon analysis are summarized in Table 2. These samples were recorded by DELPHI during 1997 to 2000. The multi-photon analysis also included data recorded during 1995 and 1996 at the centre-of-mass energies of 130, 136, 161 and 172 GeV. These samples added another 21 pb$^{-1}$ of integrated luminosity.

| Year | $\sqrt{s}$ (GeV) | | Luminosity (pb$^{-1}$) | | |
|------|------|---------|------|------|------|
|      | bin  | average | HPC  | FEMC | STIC |
| 1997 | 180.8-184.0 | 182.7 | 50.2  | 49.2  | 51.4  |
| 1998 | 188.3-189.2 | 188.6 | 154.7 | 157.7 | 157.3 |
| 1999 | 191.4-191.8 | 191.6 | 25.9  | 25.9  | 25.9  |
| 1999 | 195.4-195.9 | 195.5 | 76.4  | 76.4  | 76.4  |
| 1999 | 199.1-200.0 | 199.5 | 83.4  | 83.4  | 83.4  |
| 1999 | 201.4-202.0 | 201.6 | 40.6  | 40.6  | 40.6  |
| 2000 | 202.0-204.5 | 203.7 | 8.4   | 8.4   | 8.4   |
| 2000 | 204.5-206.0 | 205.2 | 76.2  | 76.3  | 76.1  |
| 2000 | 206.0-207.5 | 206.7 | 121.6 | 125.7 | 125.6 |
| 2000 | 207.5-209.2 | 208.2 | 8.3   | 8.4   | 8.4   |

Table 2: The different datasets used in the single-photon analysis.

## 4.2 Simulation of the Standard Model background

### 4.2.1 The single-photon analysis

Apart from the $e^+e^- \rightarrow \nu\bar{\nu}\gamma(\gamma)$ process, single-photon events can be faked by the QED reaction $e^+e^- \rightarrow e^+e^-\gamma$ if the two electrons escape undetected along the beampipe or if the electrons are in the detector acceptance but are not detected by the experiment.

This process has a very high cross-section, decreasing rapidly when the energy ($E_\gamma$) and the polar angle ($\theta_\gamma$) of the photon increase. The behaviour of this QED background together with the rapidly varying efficiencies at low energies are the reasons why different energy cuts had to be applied to photons in the three calorimeters: $x_\gamma > 0.06$ (HPC), $x_\gamma > 0.10$ (FEMC) and $x_\gamma > 0.30$ (STIC). The energy-dependent cut on the polar angle in the FEMC and STIC analyses were also necessary to reduce this background. Another critical parameter in the rejection was the polar angle at which the electrons start being seen in the STIC detector. This detector reconstructs electrons down to $\theta = 2.2°$ and in addition, the scintillator counters mounted on the beampipe could be used to reject events with electrons down to 1.8°. Simulations have shown that even at lower angles (down to 0.97°) a large fraction of the electrons were detectable because they interacted with a tungsten shield mounted inside the beampipe and leaked enough energy into the STIC to make it possible to reject the events.

The remaining background from the $e^+e^-\gamma$ process was calculated with a Monte Carlo program [18] and two different event topologies were found to contribute. Either both electrons were below the STIC acceptance or one of the electrons was in the DELPHI

acceptance where it was wrongly identified as a photon, while the photon was lost in the holes between the electromagnetic calorimeters. The first topology gives background at low photon energy while the second one produces fake photon events at high energy.

In the STIC analysis, an additional background was due to the single electrons produced by interactions between the beam particles and residual gas molecules in the LEP beampipe. In these $e \to e\gamma$ events, the photons were always lost in the beampipe while the off-energy electrons were bent into the STIC acceptance by the low-beta quadrupoles close to the DELPHI experiment. The rate of this background was so large that it was not possible to provide a $\gamma - e$ separation powerful enough to eliminate it completely. A simulation has been made of off-energy electron production [19], but it could not be used in the analysis since the vacuum pressure around the LEP ring was not known to the required precision. Instead, a background sample was collected with a trigger similar to the photon trigger except that it did not use the scintillators for photon-electron separation. After applying all the cuts used in the single-photon analysis, except the scintillator requirements, this background sample was used to estimate the remaining off-energy electron background and 19% of the overall background was estimated to be caused by off-energy electrons.

The contributions from other processes such as $\gamma\gamma$ collisions [20], $e^+e^- \to \gamma\gamma(\gamma)$ [21], cosmic ray events, $e^+e^- \to \mu^+\mu^-\gamma$ [17], $e^+e^- \to \tau^+\tau^-\gamma$ [17] and four-fermion events [22] have also been calculated.

The $\nu\bar{\nu}\gamma(\gamma)$ process was simulated by the KORALZ [17] program. Comparisons of the predicted cross-section by KORALZ 4.02 has been made with the cross-section predicted by the NUNUGPV [23] and KK 4.19 [24] programs. The total cross-section in the STIC, FEMC and HPC acceptance was calculated to be 1.0% lower by the KK program than by the KORALZ program. In the acceptance relevant to most searches, i.e., for events with a photon with $x_\gamma < 0.70$ in the FEMC or the HPC, KK predicted a cross-section that was 1% lower than the prediction by KORALZ. The NUNUGPV program has earlier been shown to give predictions within 1% of those of the KORALZ program [5] in measurements using the full energy range of the photons. These theoretical uncertainties are insignificant compared to the statistical and systematic uncertainties in the present measurement.

### 4.2.2   The multi-photon analysis

Multi-photon final states can be produced at LEP via the reactions $e^+e^- \to \nu\bar{\nu}\gamma\gamma(\gamma)$ and $e^+e^- \to \gamma\gamma(\gamma)$. In the case of double ISR with final state $\nu\bar{\nu}$ production, the photons tend to have a relatively low transverse momentum and tend to have both large acoplanarity and large acollinearity. Since the neutrino production is mainly mediated by Z-exchange in the s-channel, the missing mass distribution has a large peak corresponding to the mass of the Z. The $e^+e^- \to \nu\bar{\nu}\gamma\gamma(\gamma)$ process was, as in the single-photon case, simulated by the KORALZ generator [17].

The process $e^+e^- \to \gamma\gamma(\gamma)$ is a QED interaction between the incoming electron and positron and it is mediated by an electron in the t-channel. The RADCOR model [21] was used to simulate this background. The process is easy to reject when only two hard photons are produced but if additional hard ISR photons are emitted and lost in the beampipe, the visible photon pair can show relatively large acollinearity but small acoplanarity.

Additional minor background contributions can come from double radiative Bhabha events $e^+e^- \to e^+e^-\gamma\gamma$ when both electrons remain undetected or from radiative Bhabha events where one or more electrons are wrongly identified as photons. The BHWIDE

program [25] was used as an event generator for these events. A requirement of a minimum transverse missing momentum very effectively eliminated the cases where both electrons escaped along the beampipe.

# 5  Comparison with Standard Model expectations

## 5.1  Single-photon cross-section

The energy spectrum of the 1526 selected single-photon events from all calorimeters is shown in Figure 1 together with the expected contributions from known sources. The $x_\gamma$ distributions are shown for three $\sqrt{s}$-bins and the integrated luminosity and average $\sqrt{s}$ of the datasets that make up these bins are given in Table 2. The $\nu\bar{\nu}\gamma$ process was simulated by the KORALZ [17] program and then passed through the extensive detector simulation package of DELPHI [13].

The missing mass (or recoil mass) distributions of the events recorded at $\sqrt{s}$=180-209 GeV are shown in Figure 2. In this plot the distributions obtained with each of the three DELPHI electromagnetic calorimeters are shown separately. Data samples recorded at different $\sqrt{s}$ extend to different maximum values of missing mass and this creates "steps" in the distributions. Events where the measured energy of the photon is larger than the collision energy have been put in the first bin. The number of these events is larger in the data than expected. The simulation of background sources show that some of these events can be explained by QED two-photon events with one of the photons escaping detection. It is possible that the excess is due to temporary problems with some calorimeter channels that were not perfectly reproduced in the simulation and which created a larger QED background in the data sample. Otherwise there is no sign of an excess above the Standard Model expectation in any of the three calorimeter analyses nor in any of the $\sqrt{s}$-bins.

The number of events and cross-sections obtained from the event samples after correcting for background and efficiencies are given in Table 3. This table does not include the FEMC events with $x_\gamma < 0.20$ since they were used only in the searches and not in the cross-section calculations. The previously mentioned Monte Carlo programs were used to calculate the expected values of the cross-section of the process $e^+e^- \to \nu\bar{\nu}\gamma(\gamma)$ inside the acceptance of each of the three detectors used in the analysis. The contributions from various sources to the systematic error in the cross-section measurement are given in Table 4. The dominant uncertainty comes from the estimation of trigger and detection efficiencies while the theoretical uncertainty is insignificant compared with the experimental systematic errors.

Figure 3 shows the expected behaviour of the Standard Model single-photon cross-section as a function of the LEP energy, compared with the values measured with the STIC, FEMC and HPC calorimeters. The Standard Model prediction, calculated by KORALZ, tends to be above the data but the difference is not statistically significant.

## 5.2  Non-pointing single-photon events and multi-photon events

The numbers of events with a single non-pointing photon or with multi-photon final states are compared to Standard Model expectations in Table 5.

The missing mass spectra for the preselected multi-photon events and the expected contribution from $e^+e^- \to \nu\bar{\nu}\gamma\gamma(\gamma)$ as simulated with KORALZ are shown in Figure 4. Additional background contributions from the processes $e^+e^- \to e^+e^-\gamma$ and $e^+e^- \to \gamma\gamma\gamma$

| | $\sqrt{s}$ | 180-190 GeV | 190-200 GeV | 200-209 GeV |
|---|---|---|---|---|
| | $< \sqrt{s} >$ | 187.1 GeV | 196.8 GeV | 205.4 GeV |
| STIC $0.3 < x_\gamma < 0.9$ $3.8° < \theta_\gamma < 8°$ $172° < \theta_\gamma < 176.2°$ | $N_{observed}$ | 126 | 90 | 114 |
| | $N_{background}$ | 10.1 | 7.2 | 7.1 |
| | $N_{e^+e^- \to \nu\bar\nu\gamma}$ | 123.8±1.2 | 86.9±1.0 | 112.9±1.7 |
| | $\sigma_{meas}$ (pb) | 1.37±0.14 | 1.22±0.14 | 1.12±0.11 |
| | $\sigma_{\nu\bar\nu\gamma(\gamma)}$ (pb) | 1.44 | 1.29 | 1.18 |
| | $N_\nu$ | 2.83±0.31 | 2.81±0.37 | 2.81±0.33 |
| FEMC $0.2 < x_\gamma < 0.9$ $12° < \theta_\gamma < 32°$ $148° < \theta_\gamma < 168°$ | $N_{observed}$ | 220 | 175 | 224 |
| | $N_{background}$ | 9.5 | 8.9 | 9.0 |
| | $N_{e^+e^- \to \nu\bar\nu\gamma}$ | 208.3±2.2 | 168.1±1.1 | 200.4±1.6 |
| | $\sigma_{meas}$ (pb) | 1.98±0.14 | 1.71±0.14 | 1.71±0.12 |
| | $\sigma_{\nu\bar\nu\gamma(\gamma)}$ (pb) | 1.97 | 1.76 | 1.57 |
| | $N_\nu$ | 3.03±0.25 | 2.90±0.28 | 3.30±0.27 |
| HPC $0.06 < x_\gamma < 1.1$ $45° < \theta_\gamma < 135°$ | $N_{observed}$ | 177 | 127 | 190 |
| | $N_{background}$ | 0.3 | 0.2 | 0.1 |
| | $N_{e^+e^- \to \nu\bar\nu\gamma}$ | 190.1±2.6 | 151.4±1.1 | 198.1±2.0 |
| | $\sigma_{meas}$ (pb) | 1.78±0.13 | 1.41±0.13 | 1.50±0.11 |
| | $\sigma_{\nu\bar\nu\gamma(\gamma)}$ (pb) | 1.89 | 1.75 | 1.61 |
| | $N_\nu$ | 2.76±0.29 | 2.18±0.30 | 2.71±0.30 |

Table 3: The number of selected and expected single-photon events and the measured and calculated cross-sections with three DELPHI calorimeters for $e^+e^- \to \nu\bar\nu\gamma(\gamma)$ (KORALZ with three neutrino generations) and the number of neutrino generations calculated from the cross-sections. The errors are statistical only.

have been estimated to be 0.43±0.16 events at the preselection level and have been added to the simulated sample. The measured missing mass distribution is in good agreement with the simulation and no significant excess over Standard Model expectations was found in any of the data samples collected at energies up to $\sqrt{s} = 209$ GeV.

# 6    Limits on new phenomena

## 6.1    Neutrino physics

### 6.1.1    Measurement of the number of light neutrino families

A measurement of the cross-section of the process $e^+e^- \to \nu\bar\nu\gamma$ determines the number of light neutrino generations, $N_\nu$. The LEP2 cross-section measurements have been compared with the expected cross-sections for 2, 3 and 4 neutrino generations, calculated with KORALZ, and the number of neutrino generations has been deduced (Table 3). Averaging the independent measurements from the three different calorimeters at $\sqrt{s} = 180-209$ GeV, the number of light neutrino generations becomes:

$$N_\nu = 2.84 \pm 0.10(stat) \pm 0.14(syst)$$

| Source | HPC Variation | HPC $\Delta\sigma$ | FEMC Variation | FEMC $\Delta\sigma$ | STIC Variation | STIC $\Delta\sigma$ |
|---|---|---|---|---|---|---|
| Luminosity | ±0.6% | ±0.6% | ±0.6% | ±0.6% | ±0.6% | ±0.6% |
| Trigger efficiency | ±5% | ±5% | ±2% | ±2% | ±6% | ±6% |
| Identification efficiency | ±5% | ±5% | ±6% | ±6% | ±5% | ±5% |
| Calorimeter energy scale | ±5% | ±4% | ±4% | ±4% | ±0.5% | ±1% |
| Background | ±57% | ±0.1% | ±55% | ±2% | ±62% | ±5% |
| Total | | ±8% | | ±8% | | ±9% |

Table 4: Contributions to systematic error in the cross-section measurement of the process $e^+e^- \to \nu\bar{\nu}\gamma$. The total systematic error is the quadratic sum of the individual errors.

| | 130-190 GeV Observed | 130-190 GeV Expected | 190-209 GeV Observed | 190-209 GeV Expected |
|---|---|---|---|---|
| Preselected multi-photon events | 27 | 25.3±1.0 | 41 | 39.3±0.8 |
| $e^+e^- \to \tilde{\chi}_1^0\tilde{\chi}_1^0 \to \tilde{G}\gamma\tilde{G}\gamma$ selection | 7 | 7.1±0.5 | 17 | 13.8±0.4 |
| $e^+e^- \to \tilde{\chi}_2^0\tilde{\chi}_2^0 \to \tilde{\chi}_1^0\gamma\tilde{\chi}_1^0\gamma$ selection | 12 | 8.6±0.6 | 14 | 15.2±0.6 |
| Non-pointing single-photon events | 6 | 7.6±0.9 | 10 | 7.0±0.7 |

Table 5: The number of observed and expected events from Standard Model sources in four selected data samples.

### 6.1.2 Neutrino interactions beyond the Standard Model

The contribution to the single-photon process $e^+e^- \to \nu\bar{\nu}\gamma$ from hypothetical Non-Standard (NS) neutrino interactions with the electron, has recently been calculated in order to set limits on theories which attempt to explain the solar and atmospheric neutrino anomalies [26]. The single-photon cross-section due to these non-standard neutrino interactions was computed at tree level in a point interaction approximation where $\epsilon_{\alpha R}$ and $\epsilon_{\alpha L}$ ($\alpha = e, \mu, \tau$) parameterise the strength, relative to the Fermi constant ($G_F$), of the non-standard interactions between the three neutrinos and the electron. The radiator approximation [27] was used in these calculations to determine the single-photon cross-section from initial state radiation.

The analysis was made for three different assumptions as suggested by [26]:

I. The NS interactions couple only to the electron neutrino, $e^+e^- \to \nu_e\bar{\nu}_e\gamma$.
II. The NS interactions couple only to the tau neutrino, $e^+e^- \to \nu_\tau\bar{\nu}_\tau\gamma$.
III. The NS interactions couple only to a flavour changing neutral current, $e^+e^- \to \nu_\alpha\bar{\nu}_\beta\gamma$ where $\alpha \neq \beta$.

The analysis was in all three cases based on the single-photon samples recorded with the HPC and FEMC detectors and the event selection was optimised with the likelihood ratio method mentioned in section 3.1.2. Under the first assumption, the interference terms between the non-standard interaction and the Standard Model amplitudes can, in some parts of the $\epsilon_{eL} - \epsilon_{eR}$ parameter space, give a negative contribution to the single-photon cross-section at a level which the analysis is sensitive enough to exclude. The analysis under the first assumption was for this reason divided into two independent

parts based on the regions of the photon energy distribution for which a positive and a negative contribution from non-standard neutrino interactions was predicted.

The calculated allowed and excluded regions in the $\epsilon_L - \epsilon_R$ planes for the three different assumptions are shown in Figure 5. To exclude a point in the $\epsilon_{eL} - \epsilon_{eR}$ plane a logical OR was used between the two analyses of positive and negative interference and this gives the "crescent moon" shape of the allowed region in Figure 5a. All limits were calculated at a 95% C.L. and the limits were computed by combining all the FEMC and HPC data samples in Table 2.

## 6.2   Limits on the production of unknown neutral states

### 6.2.1   Limits on $e^+e^- \to X\gamma$ production

The observed single-photon events have been used to set a limit on the production cross-section of a new hypothetical particle, X, produced in association with an ISR photon and being stable or decaying to invisible decay products. The upper limits for the cross-section of the process $e^+e^- \to \gamma + X$ were calculated from the missing mass distribution (Figure 6) at $\sqrt{s} = 200 - 209$ GeV (average $\sqrt{s} = 205.4$ GeV) of the 190 events in the angular region $45° - 135°$ and the 414 single $\gamma$ events in the angular region $12° - 168°$ while taking into account the expected background. The limits are valid if the intrinsic width of the $X$ particle is negligible compared to the detector resolution (the recoil mass resolution varies between 10 GeV/c$^2$ at the $Z^0$ peak to 1 GeV/c$^2$ at high masses). Separate 95% C.L. upper limits are given in Figure 6 for photons in the HPC region and in the FEMC+HPC region. In the latter case an assumption of an ISR-like photon angular distribution has been made to correct for losses between the calorimeters.

### 6.2.2   Limits on $e^+e^- \to XY \to YY\gamma$ production

A cross-section limit has been calculated for the scenario where hypothetical $X$- and $Y$-particles are produced and the $X$-particle decays into a $Y$ and a photon, $e^+e^- \to XY \to YY\gamma$. It is assumed that the $Y$ particles escape detection (such as in the process $e^+e^- \to \tilde{\chi}_2^0\tilde{\chi}_1^0 \to \tilde{\chi}_1^0\tilde{\chi}_1^0\gamma$ which is predicted by certain SUSY models) and that the branching ratio of $X \to Y\gamma$ is 100% .

It is, in addition, assumed that the $E_\gamma$ and $\cos\theta_\gamma$ distributions are flat. This assumption results in a very small predicted signal within the STIC acceptance and for this reason only the single-photon events recorded by the HPC and FEMC detectors were used in this analysis. The data collected at $\sqrt{s}$=199-209 GeV (average $\sqrt{s}$ =204.0 GeV) were used in the analysis and it was assumed that any $\sqrt{s}$-dependence of the signal would be insignificant in this limited $\sqrt{s}$-range. The analysis has been performed at 401 points in the mass plane of the $X$ and $Y$ particles where the selection cuts have been optimised at every point with a likelihood ratio method. The obtained and expected cross-section limits, within the HPC + FEMC acceptance, in the mass plane of the $X$ and $Y$ particles are shown in Figure 7.

## 6.3   Limits on the production of gravitons

If there are extra compact dimensions of space in which only gravity can propagate, gravitational interactions could be unified with gauge interactions already at the weak scale [7,8]. The consequence of this model is that at LEP gravity could manifest itself

by the production of gravitons $(G)$, which themselves would be undetectable by the experiments. Instead single photons from the $e^+e^- \to \gamma G$ reaction could be observable.

In these gravitational models, a fundamental mass scale, $M_D$, is introduced, which is related to the gravitational constant $G_N$ and to the size or radius $R$ of the compactified space (assumed to be a torus) by $M_D^{n+2} R^n = (4\pi G_N)^{-1}$ [7] or $M_D^{n+2} R^n = (8\pi G_N)^{-1}$ [8] where $n$ is the number of dimensions in addition to the usual 3+1-dimensional space[3].

With one extra dimension and a fundamental scale of 0.5-1 TeV, the size of this dimension becomes $10^{12} - 10^{13}$ m which is excluded by macroscopic measurements. However, already with two extra dimensions, $R$ is in the range 0.5-2 mm and with $n=6$ the size of the dimensions becomes 30-70 fm. In this case the modification of the gravitational force would not have been observed in previous gravitational measurements.

The differential cross-section for the $e^+e^- \to \gamma G$ process has been calculated in [8]. Initial state radiation can produce additional photons that would cause a signal event to be rejected in a single-photon analysis. The expected signal cross-section has therefore been corrected with a radiator approximation method [27].

From Figure 2 it is clear that only a very small signal can be expected in the STIC detector compared with the one in the FEMC and the HPC. For this reason only the latter two detectors were used in this analysis. All DELPHI data with $\sqrt{s} > 180$ GeV were used and for each bin in $\sqrt{s}$ (see Table 2) a limit was calculated after a cut optimisation based on a likelihood ratio method as described in section 3.1.2. These limits were then combined to give a 95% C.L. cross-section limit at 208 GeV of 0.14 pb for 2 and 4 extra dimensions. The resulting limits on the fundamental mass scale are $M_D > 1.31$ TeV/c$^2$ for $n=2$ and $M_D > 0.82$ TeV/c$^2$ for $n=4$ (Figure 8). This in turn can be transformed into a limit on the size (radius) of the extra dimensions which is $R < 0.27$ mm and $R < 13$ pm for 2 and 4 extra dimensions respectively. Limits for other numbers of extra dimensions are given in Table 6. The systematic error on the $M_D$ limits is estimated to be between 1% and 2% .

| Dimensions | $\sigma_{Limit}$ (pb) | $M_D$ (expected) | $M_D$ (obtained) | Radius |
|------------|------------------------|-------------------|-------------------|---------|
| 2 | 0.14 | >1.27 TeV/c$^2$ | >1.31 TeV/c$^2$ | <0.27 mm |
| 3 | 0.14 | >0.98 TeV/c$^2$ | >1.02 TeV/c$^2$ | <3.5 nm |
| 4 | 0.14 | >0.80 TeV/c$^2$ | >0.82 TeV/c$^2$ | <13 pm |
| 5 | 0.17 | >0.67 TeV/c$^2$ | >0.67 TeV/c$^2$ | <0.49 pm |
| 6 | 0.18 | >0.58 TeV/c$^2$ | >0.58 TeV/c$^2$ | <55 fm |

Table 6: Limits at the 95% confidence level on the fundamental mass scale $M_D$ and the radius for different numbers of extra dimensions.

## 6.4   SUSY particles

### 6.4.1   Limits on the gravitino mass

The cross-section for the process $e^+e^- \to \tilde{G}\tilde{G}\gamma$ has been computed under the assumption that all other supersymmetric particles are too heavy to be produced [10]. The largest sensitivity in this type of search is obtained with photons at low energy and low polar angle. Since the signal cross-section grows as the sixth power of the centre-of-mass energy, the highest sensitivity is also obtained at the highest available beam energy.

---

[3]Note that the definition of $M_D$ in [7] is a factor $2^{1/(n+2)}$ larger than in [8] and that the limits presented here are for an $M_D$ as defined by [8].

Lower limits on the mass of a gravitino produced by the $e^+e^- \rightarrow \tilde{G}\tilde{G}\gamma$ process have been extracted previously at LEP [5,6].

The expected signal cross-section in [10] has in the present study been corrected for initial state radiation [27] that produces multi-photon events which are rejected in the analysis. The large energy cut in the STIC analysis meant that this detector did not contribute significantly to the results. Limits were therefore calculated for only the FEMC and HPC data in the ten $\sqrt{s}$ bins of Table 2 and after a similar combination of these limits as in the graviton analysis, a 95% C.L. limit of $\sigma < 0.18$ pb at 208 GeV was obtained. This corresponds to a lower limit on the gravitino mass which is

$$m_{\tilde{G}} > 1.09 \cdot 10^{-5} \text{ eV/c}^2 \quad \text{at 95\% C.L.}$$

while the expected limit is $1.10 \cdot 10^{-5}$ eV/c$^2$. The systematic error on the $m_{\tilde{G}}$ limit is estimated to be 2% . Since the supersymmetry-breaking scale $|F|^{\frac{1}{2}}$ is related to the gravitino mass and the gravitational constant $(G_N)$ by $|F| = \sqrt{\frac{3}{8\pi}/G_N} \cdot m_{\tilde{G}}$, the limit on this scale is $|F|^{\frac{1}{2}} > 214$ GeV.

### 6.4.2 Limits on neutralino production if the $\tilde{G}$ is the LSP

Supersymmetric models such as the gauge-mediated supersymmetric model [9] or the no-scale supergravity model [12] (LNZ) predict that the gravitino $\tilde{G}$ is the lightest supersymmetric particle (LSP). If the next-to-lightest supersymmetric particle (NLSP) is the neutralino $\tilde{\chi}_1^0$, both single-photon and multi-photon production can occur at LEP2 via the processes $e^+e^- \rightarrow \tilde{G}\tilde{\chi}_1^0 \rightarrow \tilde{G}\tilde{G}\gamma$ and $e^+e^- \rightarrow \tilde{\chi}_1^0\tilde{\chi}_1^0 \rightarrow \tilde{G}\gamma\tilde{G}\gamma$. While the rate of the former process is proportional to the inverse of the gravitino mass squared, the two-photon process is independent of the gravitino mass. Consequently, the single-photon process is expected to dominate only for ultra light gravitinos.

The expected photon distributions from the process $e^+e^- \rightarrow \tilde{G}\tilde{\chi}_1^0 \rightarrow \tilde{G}\tilde{G}\gamma$ were generated with SUSYGEN [28], and the event selection was optimised with a likelihood ratio method. The same analysis was repeated at 26 different neutralino masses $(m_{\tilde{\chi}_1^0})$ between 80 and 208 GeV/c$^2$. The 95% C.L. cross-section limit for $e^+e^- \rightarrow \tilde{G}\tilde{\chi}_1^0 \rightarrow \tilde{G}\tilde{G}\gamma$ production was computed at 208 GeV after combining the limits from the single-photon data recorded with the FEMC and HPC detectors at a $\sqrt{s}$ between 180 and 209 GeV, assuming the signal cross-section to scale as $\beta^8$ (where $\beta$ is the neutralino velocity).

The analysis was applied to two different theoretical scenarios. In the first one, the neutralino was assumed to be a pure bino and the right- and left-handed selectrons were degenerate in mass. Figure 9a shows the cross-section limit within the FEMC + HPC acceptance assuming that the branching ratio $Br(\tilde{\chi}_1^0 \rightarrow \tilde{G}\gamma) = 100\%$ . The exclusion regions in the $m_{\tilde{\chi}_1^0}$-$m_{\tilde{G}}$ mass plane are depicted in Figure 9b for the selectron masses $m_{\tilde{e}} = 75$ GeV/c$^2$ and $m_{\tilde{e}} = 150$ GeV/c$^2$. The branching ratios for $\tilde{\chi}_1^0 \rightarrow Z\gamma$ and $\tilde{\chi}_1^0 \rightarrow \tilde{e}e \rightarrow \tilde{G}e^+e^-$, as predicted by SUSYGEN, were taken into account in the calculation of the exclusion regions. These branching ratios affected in a significant way only the limit at low neutralino masses under the $m_{\tilde{e}} = 75$ GeV/c$^2$ assumption.

The second scenario was the no-scale supergravity model where the selectron masses and the neutralino composition depend on the neutralino mass. The no-scale supergravity model predicts a very light gravitino and the cross-section limit and the exclusion region for this model in the $m_{\tilde{\chi}_1^0}$ versus $m_{\tilde{G}}$ mass plane are shown in Figure 9c.

In the search for $e^+e^- \rightarrow \tilde{\chi}_1^0\tilde{\chi}_1^0 \rightarrow \tilde{G}\gamma\tilde{G}\gamma$ at $\sqrt{s} = 190\text{-}209$ GeV, 17 events were observed with 13.8 expected from Standard Model sources. This brings the total number of events

found at $\sqrt{s}$ =130-209 GeV to 24 with 20.9 expected (Table 5). Figure 10 shows the cross-section limit [29] calculated from these events as a function of the $\tilde{\chi}_1^0$ mass (assuming a branching ratio of 100% for $\tilde{\chi}_1^0 \to \tilde{G}\gamma$) and the exclusion region in the $m_{\tilde{\chi}}$ versus $m_{\tilde{e}_R}$ plane. A total systematic uncertainty of $\pm 5\%$ was assumed for the signal efficiency, which included the uncertainties on the signal simulation ($\pm 4\%$) and on the trigger efficiency ($\pm 3\%$). This was taken into account in deriving the cross-section limit but it had a negligible effect on the result.

The dependence of the signal cross-section on the selectron mass in Figure 10 is due to the possibility of t-channel selectron exchange in the production mechanism. A lower limit of 96 GeV/c$^2$ (100 GeV/c$^2$) at 95% C.L. for the $\tilde{\chi}_1^0$ mass can be deduced under the assumption that the neutralino is a pure bino and with the hypotheses $m_{\tilde{e}_R} = m_{\tilde{e}_L} = 2m_{\tilde{\chi}}$ ($m_{\tilde{e}_R} = m_{\tilde{e}_L} = 1.1 m_{\tilde{\chi}}$).

If the gravitino mass is larger than 200-300 eV/c$^2$, the $\tilde{\chi}_1^0$ can have such a long lifetime that it will decay far from the production point yet within the detector. The signature for this case is photons that do not point to the interaction region. If the decay length is long, the probability to detect both photons is small and it is more efficient to search for the signal events in a non-pointing single-photon sample. In this analysis it was therefore required that the photon had a shower axis reconstructed in the HPC which gave a beam crossing point at least 40 cm away from the interaction point. Ten events were found at 190-209 GeV with 7.0 expected, bringing the total at all energies to 16 with 14.6 expected from Standard Model sources (Table 5).

Figure 11 shows the cross-section limit as a function of the mean decay path of the neutralino from the non-pointing single-photon events. The limit was calculated under the assumptions that the neutralino is a pure Bino, produced dominantly via right-handed selectron t-channel exchange and that it decays isotropically to $\tilde{G}\gamma$. The ratio $m_{\tilde{e}}/m_{\tilde{\chi}}$ was furthermore assumed to be between 1.1 and 2.0 and no significant difference in signal efficiency was observed within this window.

### 6.4.3  Limits on neutralino production if the $\tilde{\chi}_1^0$ is the LSP

In other SUSY models [11] the $\tilde{\chi}_1^0$ is the LSP and $\tilde{\chi}_2^0$ is the NLSP. The $e^+e^- \to \tilde{\chi}_2^0\tilde{\chi}_2^0 \to \tilde{\chi}_1^0\gamma\tilde{\chi}_1^0\gamma$ process has an experimental signature which is the same as for $e^+e^- \to \tilde{\chi}_1^0\tilde{\chi}_1^0 \to \tilde{G}\gamma\tilde{G}\gamma$ but with somewhat different kinematics due to the masses of the $\tilde{\chi}_1^0$ and $\tilde{\chi}_2^0$. The previous DELPHI analyses at lower energies [5,4] have now been repeated with the 190-209 GeV data sample. 14 events remain after all cuts, with 15.2 expected from the Standard Model background (Table 5). The total number of events found at $\sqrt{s}$ =130-209 GeV was 26 with 23.8 expected. The expected photon distributions from $\tilde{\chi}_1^0$ were again predicted by SUSYGEN, giving a flat distribution in $cos(\theta)$ and in energy, with minimum and maximum energies which depended on the masses of the particles involved in the reaction (and on $\sqrt{s}$).

Figure 12 shows the observed and expected cross-section limits calculated from the events collected at all energies as a function of the $\tilde{\chi}_1^0$ and $\tilde{\chi}_2^0$ masses, assuming a branching ratio of 100% for $\tilde{\chi}_2^0 \to \tilde{\chi}_1^0\gamma$.

## 7  Conclusions

The DELPHI experiment has analysed all single- and acoplanar multi-photon events collected during 1995-2000 at a centre-of-mass energy between 130-209 GeV.

The measured single- and multi-photon cross-sections are in agreement with the expectations from the Standard Model process $e^+e^- \to \nu\bar{\nu}\gamma(\gamma)$ and the number of light neutrino generations was measured to be $N_\nu = 2.84 \pm 0.10(stat) \pm 0.14(syst)$.

The absence of an excess of events has been used to set model-independent limits on the production of new neutral states, a light gravitino and neutralinos.

New limits on the gravitational scale and on non-standard model interactions have also been determined.

# Acknowledgements

# References

[1] DELPHI Collaboration, P. Abreu *et al.*, Z. Phys. **C74** (1997) 577.
[2] DELPHI Collaboration, P. Abreu *et al.*, Phys. Lett. **B380** (1996) 471.
[3] DELPHI Collaboration, P. Abreu *et al.*, Eur. Phys. J. **C1** (1998) 1.
[4] DELPHI Collaboration, P. Abreu *et al.*, Eur. Phys. J. **C6** (1999) 371.
[5] DELPHI Collaboration, P. Abreu *et al.*, Eur. Phys. J. **C17** (2000) 53.
[6] ALEPH Collaboration, R. Barate *et al.*, Phys. Lett. **B420** (1998) 127;
    ALEPH Collaboration, R. Barate *et al.*, Phys. Lett. **B429** (1998) 201;
    ALEPH Collaboration, A. Heister *et al.*, Eur. Phys. J. **C28** (2003) 1;

L3 Collaboration, M. Acciarri *et al.*, Phys. Lett. **B415** (1997) 299;
L3 Collaboration, M. Acciarri *et al.*, Phys. Lett. **B444** (1998) 503;
L3 Collaboration, M. Acciarri *et al.*, Phys. Lett. **B470** (1999) 268;
L3 Collaboration, P. Achard *et al.*, Phys. Lett. **B587** (2004) 16;
OPAL Collaboration, K. Ackerstaff *et al.*, Phys. Lett. **B391** (1997) 210;
OPAL Collaboration, K. Ackerstaff *et al.*, Eur. Phys. J. **C2** (1998) 607;
OPAL Collaboration, G. Abbiendi *et al.*, Eur. Phys. J. **C8** (1999) 23;
OPAL Collaboration, G. Abbiendi *et al.*, Eur. Phys. J. **C18** (2000) 253.

 [7] N. Arkani-Hamed, S. Dimopoulos and G. Dvali, Phys. Lett. **B429** (1998) 263;
E.A. Mirabelli, M. Perelstein and M.E. Peskin, Phys. Rev. Lett. **82** (1999) 2236.

 [8] G.F. Giudice, R. Rattazzi and J.D. Wells, Nucl. Phys. **B544** (1999) 3.

 [9] S. Dimopoulos *et al.*, Phys. Rev. Lett. **76** (1996) 3494;
S. Dimopoulos *et al.*, Nucl. Phys. **B488** (1997) 39;
S. Ambrosanio *et al.*, Phys. Rev. **D54** (1996) 5395;
S. Ambrosanio *et al.*, Phys. Rev. **D56** (1997) 1761.

[10] A. Brignole, F. Feruglio and F. Zwirner, Nucl. Phys. **B516** (1998) 13;
Erratum-ibid. **B555** (1999) 653.

[11] S. Ambrosanio and B. Mele, Phys. Rev. **D52** (1995) 3900;
S. Ambrosanio and B. Mele, Phys. Rev. **D53** (1996) 2541;
S. Ambrosanio *et al.*, Nucl. Phys. **B478** (1996) 46;
S. Ambrosanio and B. Mele, Phys. Rev. **D55** (1997) 1399;
Erratum-ibid. **D56** (1997) 3157;
G.L. Kane and G. Mahlon, Phys. Lett. **B408** (1997) 222.

[12] J.L. Lopez, D.V. Nanopoulos and A. Zichichi, Phys. Rev. Lett. **77** (1996) 5168;
J.L. Lopez, D.V. Nanopoulos and A. Zichichi, Phys. Rev. **D55** (1997) 5813.

[13] DELPHI Collaboration, P. Aarnio *et al.*, Nucl. Inst. and Meth. **A303** (1991) 233;
DELPHI Collaboration, P. Abreu *et al.*, Nucl. Inst. and Meth. **A378** (1996) 57.

[14] S.J. Alvsvaag *et al.*, Nucl. Inst. and Meth. **A425** (1999) 106.

[15] T.W. Anderson, An introduction to multivariate analysis, New York Wiley, 1958.

[16] V.F. Obraztsov, Nucl. Inst. and Meth. **A316** (1992) 388;
Erratum-ibid. **A399** (1997) 500.

[17] S. Jadach, B.F.L. Ward and Z. Was, Comp. Phys. Comm. **66** (1991) 276;
S. Jadach, B.F.L. Ward and Z. Was, Comp. Phys. Comm. **79** (1994) 503.

[18] D. Karlen, Nucl. Phys. **B289** (1987) 23.

[19] E. Falk, V. Hedberg and G. von Holtey, CERN SL/97-04(EA).

[20] T. Sjöstrand *et al.*, Comp. Phys. Comm. **135** (2001) 238;
F.A. Berends, P.H. Daverveldt and R. Kleiss, Comp. Phys. Comm. **40** (1986) 271, 285 and 309;
T. Alderweireld *et al.*, CERN Report 2000-009, p219 (2000), edited by G. Passarino, R. Pittau and S. Jadach.

[21] F.A. Berends and R. Gastmans, Nucl. Phys. **B61** (1973) 414;
F.A. Berends and R. Kleiss, Nucl. Phys. **B186** (1981) 22;
F.A. Berends *et al.*, Nucl. Phys. **B239** (1984) 395.

[22] F.A. Berends, R. Pittau and R. Kleiss, Comp. Phys. Comm. **85** (1995) 437;
J. Fujimoto *et al.*, Comp. Phys. Comm. **100** (1997) 128.

[23] G. Montagna *et al.*, Nucl. Phys. **B452** (1995) 161;
G. Montagna *et al.*, Nucl. Phys. **B541** (1999) 31.

[24] S. Jadach, B.F.L. Ward and Z. Was, Comp. Phys. Comm. **130** (2000) 260.

[25] S. Jadach, W. Placzek and B.F.L. Ward, Phys. Lett. **B390** (1997) 298.

[26] Z. Berezhiani and A. Rossi, Phys. Lett. **B535** (2002) 207.

[27] O. Nicrosini and L. Trentadue, Nucl. Phys. **B318** (1989) 1.

[28] S. Katsanevas and P. Morawitz, Comp. Phys. Comm. **112** (1998) 227.

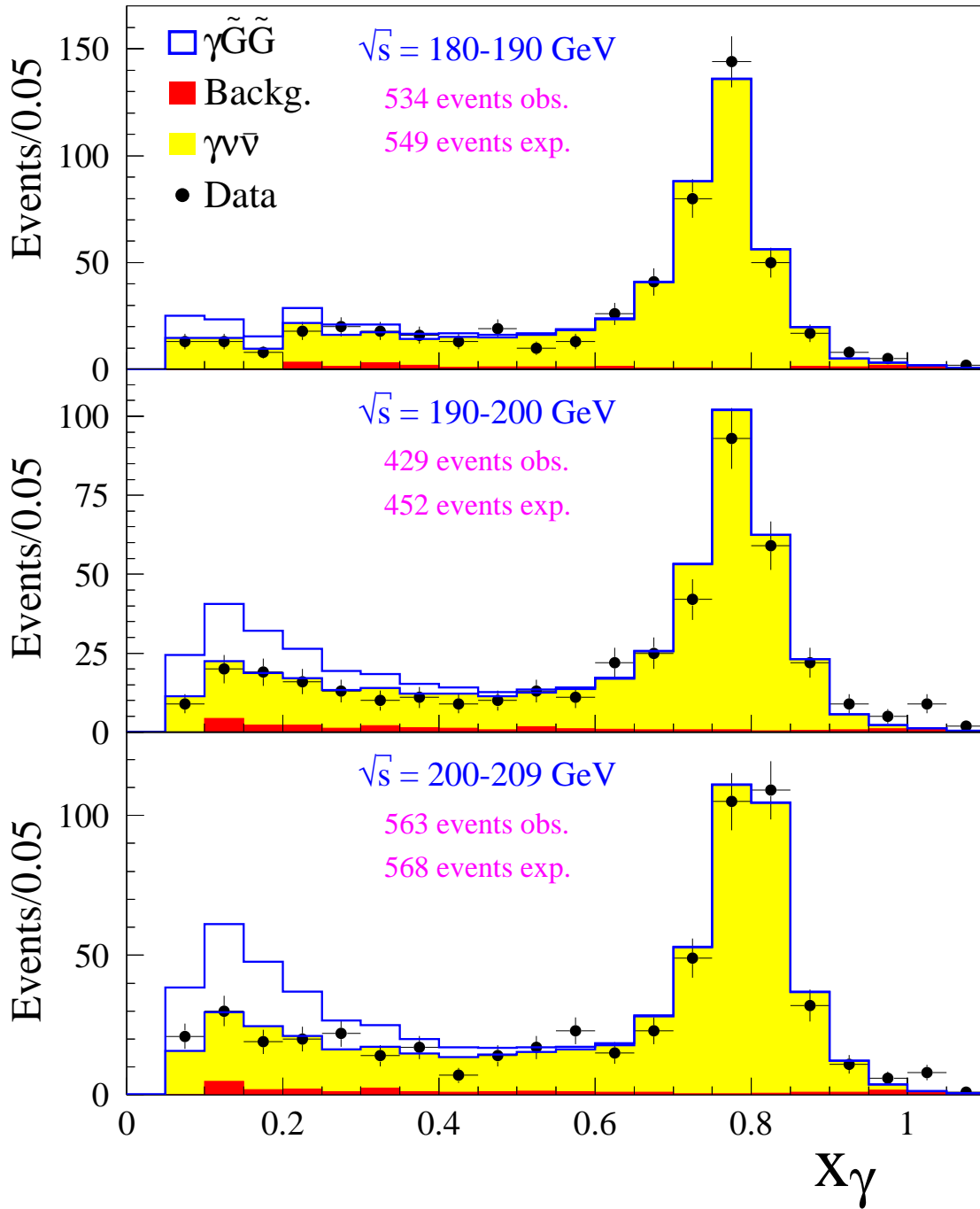[29] A.L. Read, CERN Report 2000-005, p81 (2000), edited by F. James, L. Lyons and Y. Perrin.

Figure 1: $x_\gamma$ of selected single photons for three $\sqrt{s}$-bins. The light shaded area is the expected distribution from $e^+e^- \to \nu\bar{\nu}\gamma$ and the dark shaded area is the total background from other sources. Indicated in the plot is also the signal expected from $e^+e^- \to \tilde{G}\tilde{G}\gamma$ under the assumption that $m_{\tilde{G}} = 7 \cdot 10^{-6}$ eV/c$^2$.
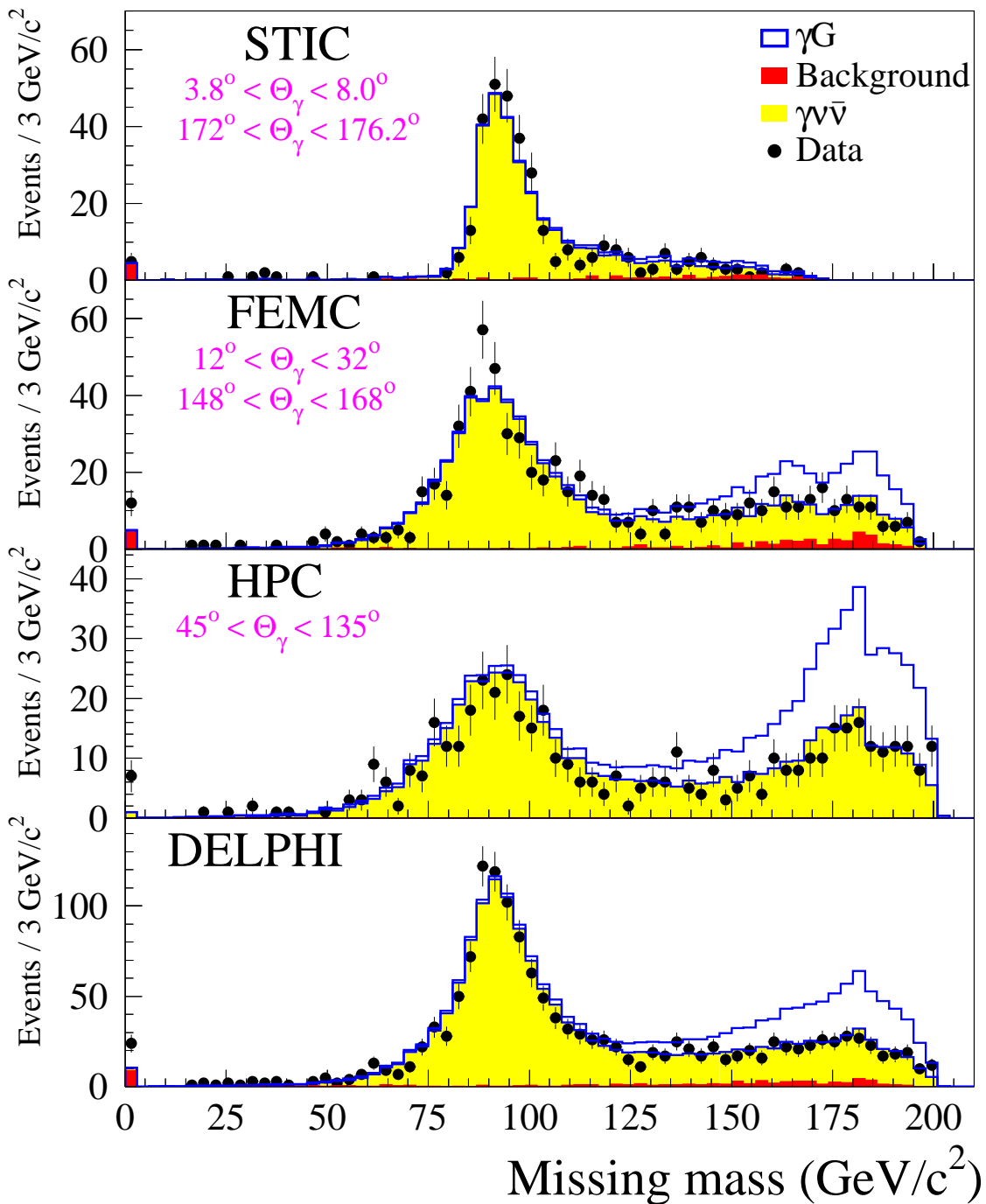
Figure 2: Missing mass (or recoil mass) distributions of all single-photon events in DELPHI (from data recorded at $\sqrt{s} = 180\text{-}209$ GeV). The figure shows the missing mass distribution from each calorimeter separately and the bottom plot shows the combined spectrum. The light shaded area is the expected distribution from $e^+e^- \to \nu\bar{\nu}\gamma$ and the dark shaded area is the total background from other sources. The signal expected from $e^+e^- \to \gamma G$ production is indicated (two extra dimensions and $M_D = 0.75$ TeV/c$^2$ were assumed in this calculation).
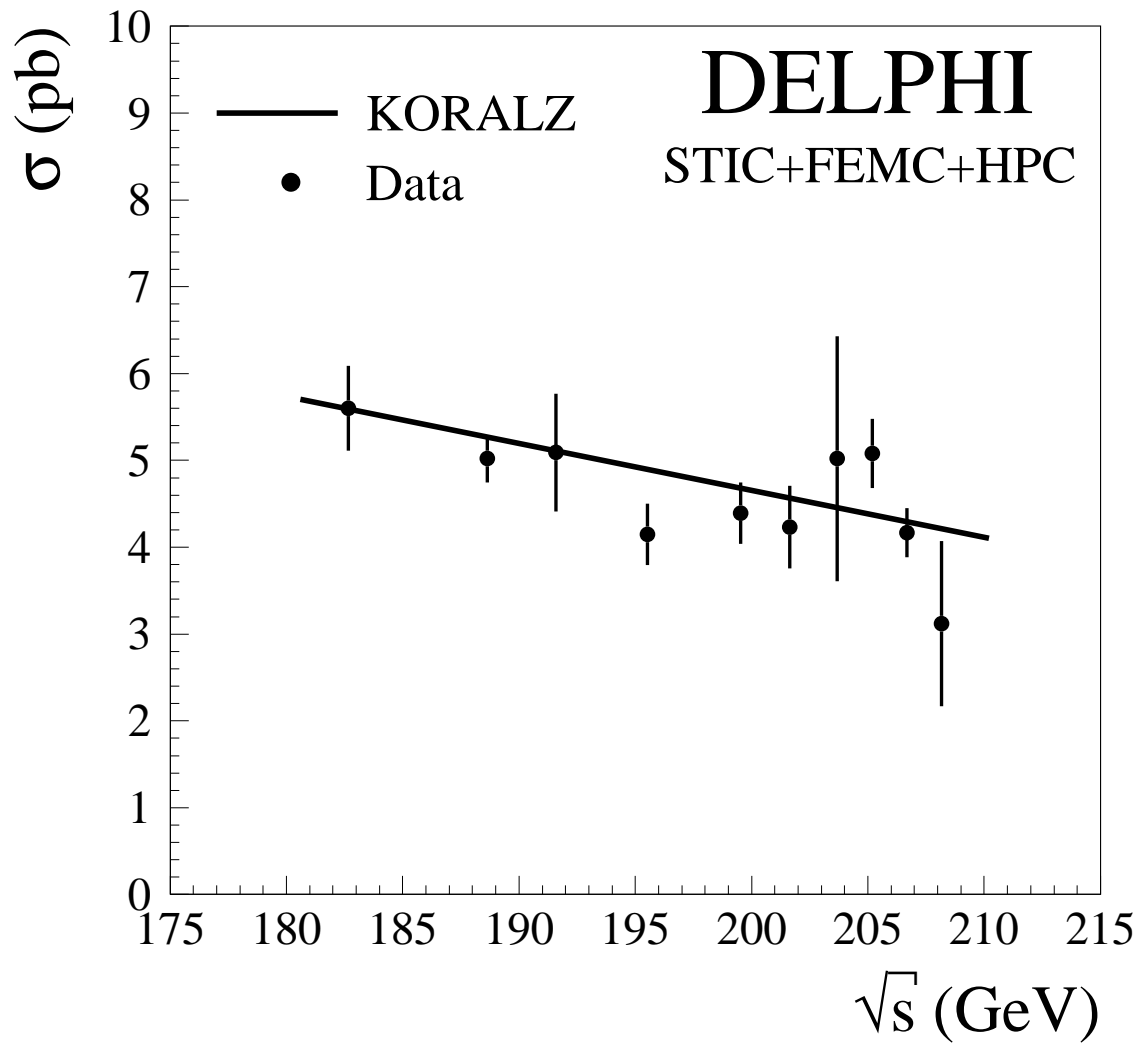
Figure 3: The single-photon cross-section measured by the STIC, FEMC and HPC detectors compared to the cross-section predicted by Koralz.
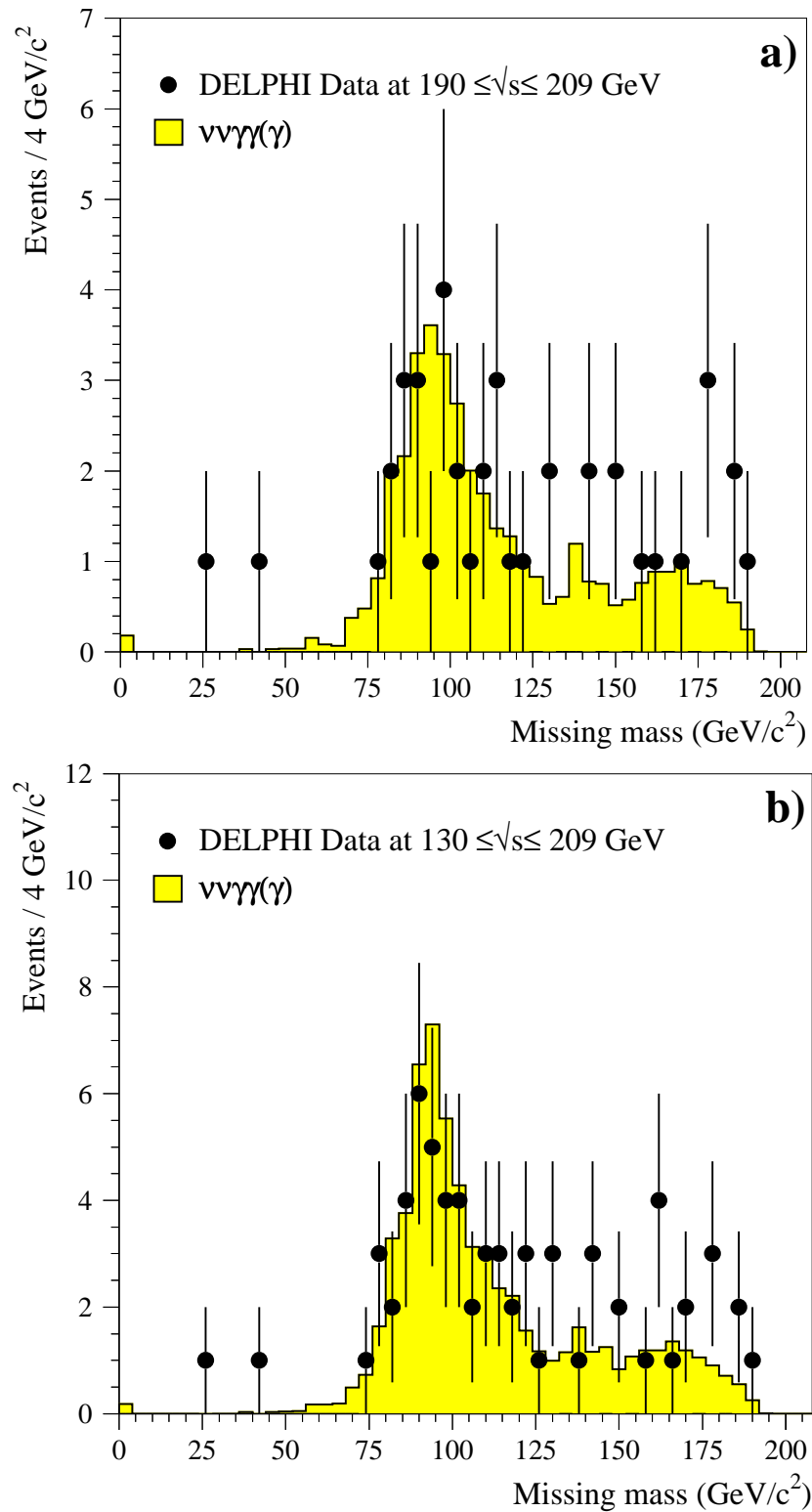
Figure 4: Missing mass distribution observed after multi-photon preselection in the 190-209 GeV sample (a) and the combined 130-209 GeV sample (b).
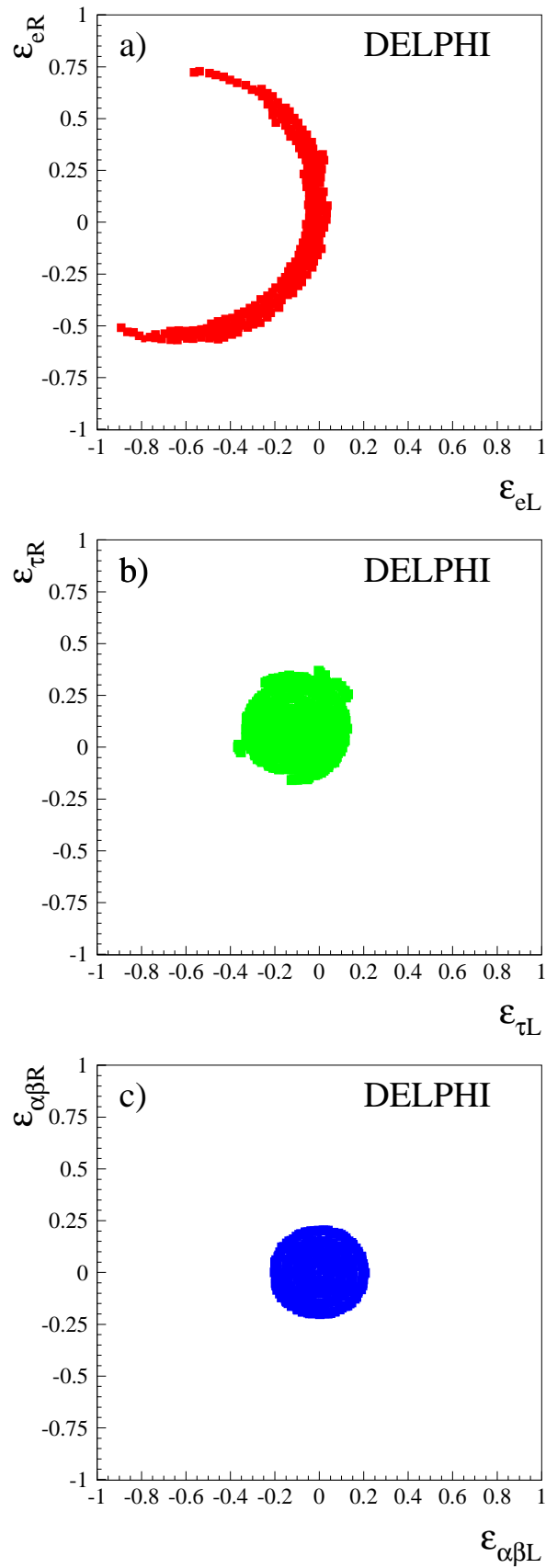
Figure 5: The remaining allowed regions. a) In the $\epsilon_{eL} - \epsilon_{eR}$ plane. b) In the $\epsilon_{\tau L} - \epsilon_{\tau R}$ plane. c) In the $\epsilon_{\alpha\beta L} - \epsilon_{\alpha\beta R}$ $(\alpha \neq \beta)$ plane.
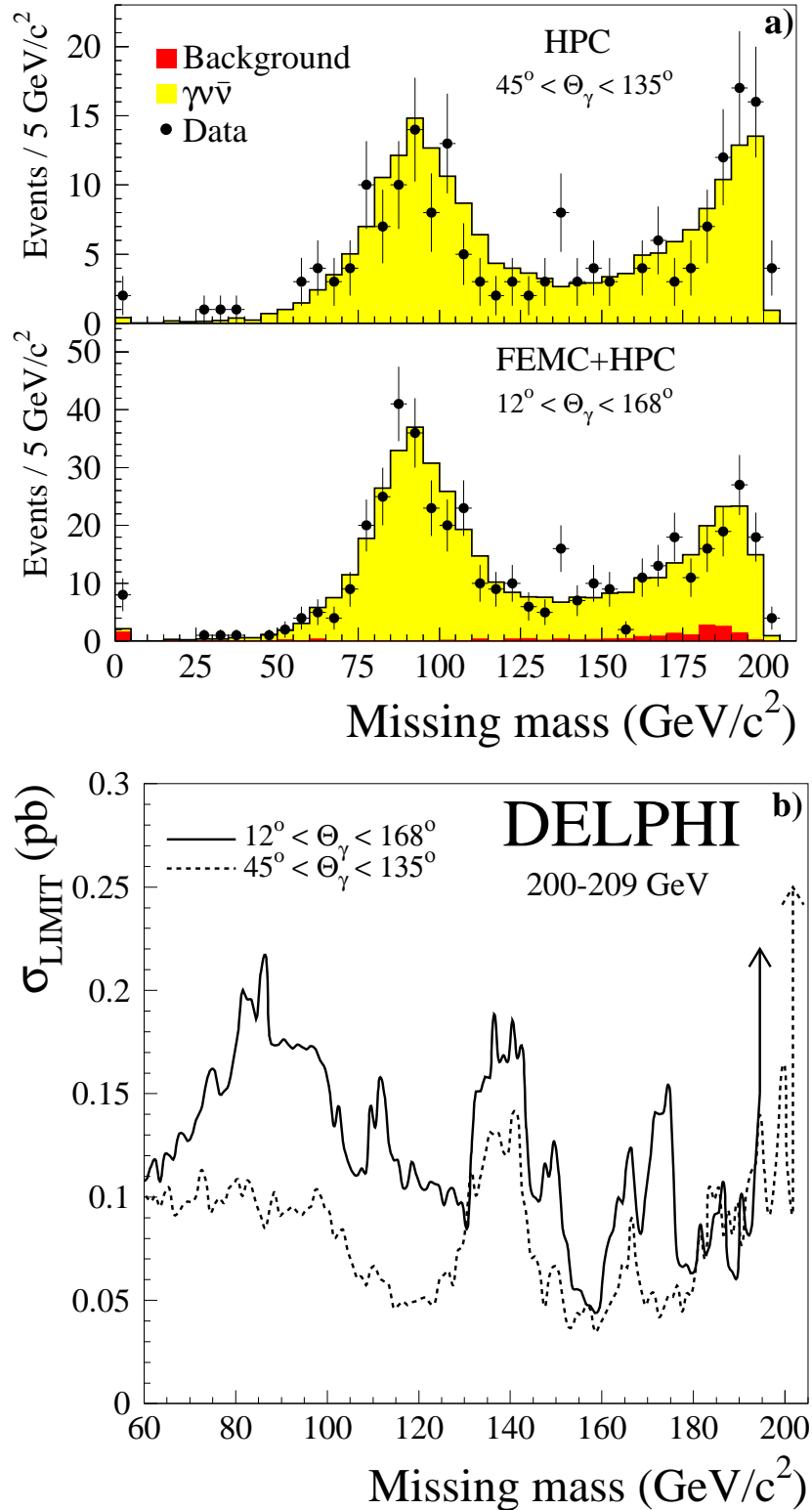
Figure 6: a) The distributions of the missing mass for the events at 200-209 GeV in the HPC and in the FEMC+HPC. The light shaded area is the expected distribution from $e^+e^- \to \nu\bar{\nu}\gamma$ and the dark shaded area is the total background from other sources. b) Upper limits at 95% C.L. and at 205 GeV (within the quoted solid angles) for the production of a new unknown stable neutral object .

# DELPHI



# DELPHI
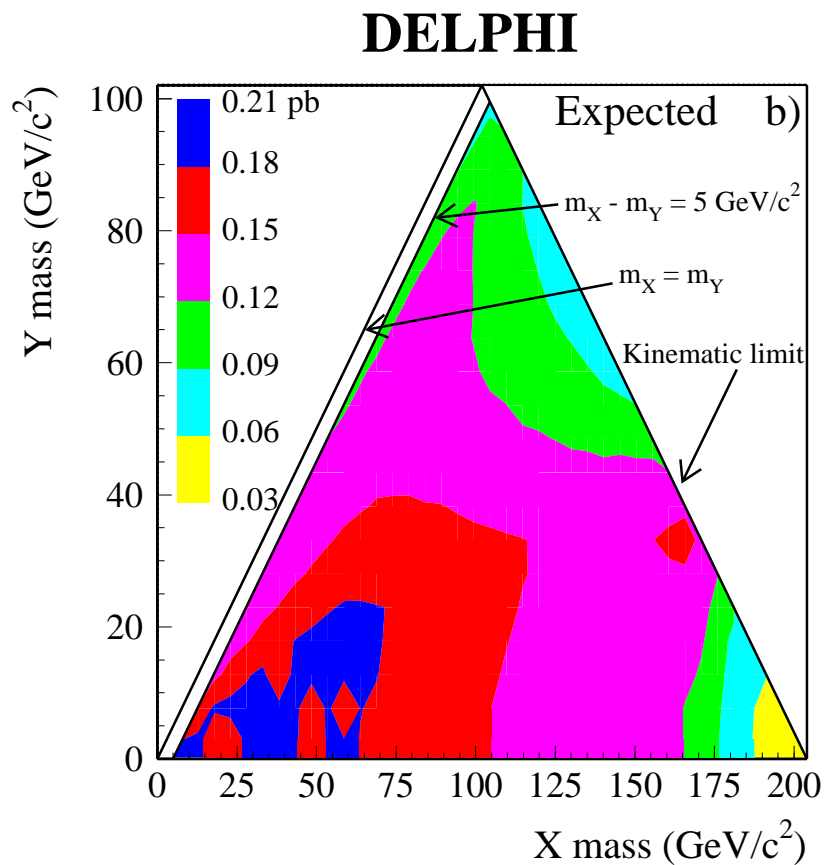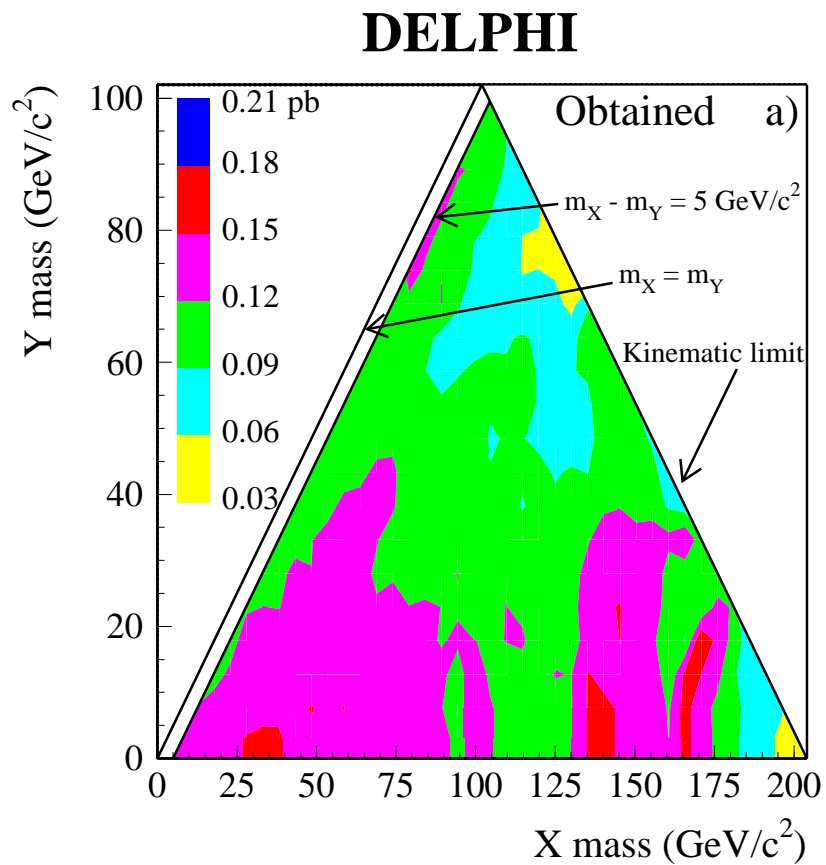


Figure 7: The obtained (a) and expected (b) cross-section limit at 95% C.L. and at 204
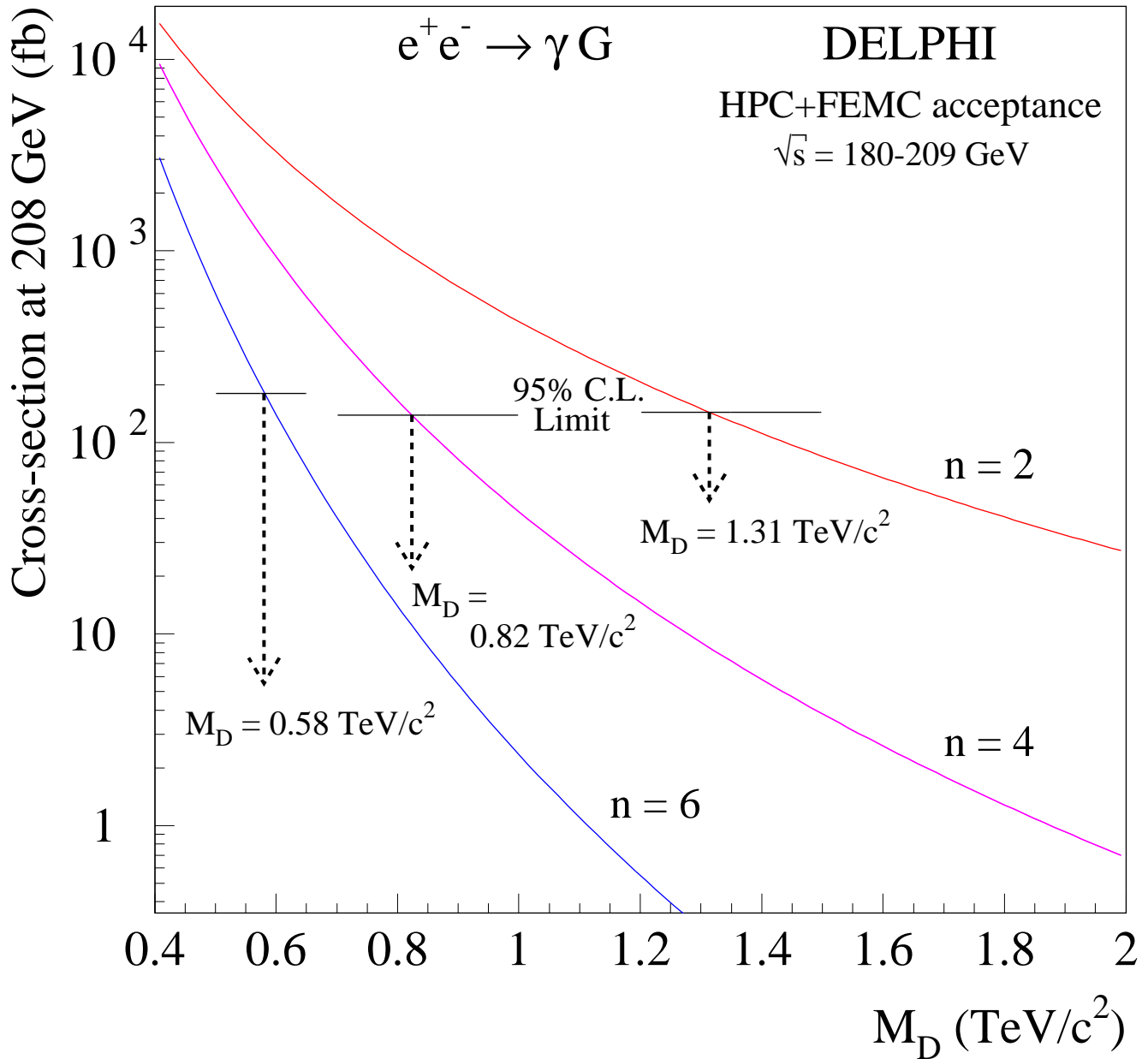
Figure 8: The cross-section limit at 95% C.L. for $e^+e^- \rightarrow \gamma G$ production at $\sqrt{s}$=208 GeV and the expected cross-section for 2, 4 and 6 extra dimensions.
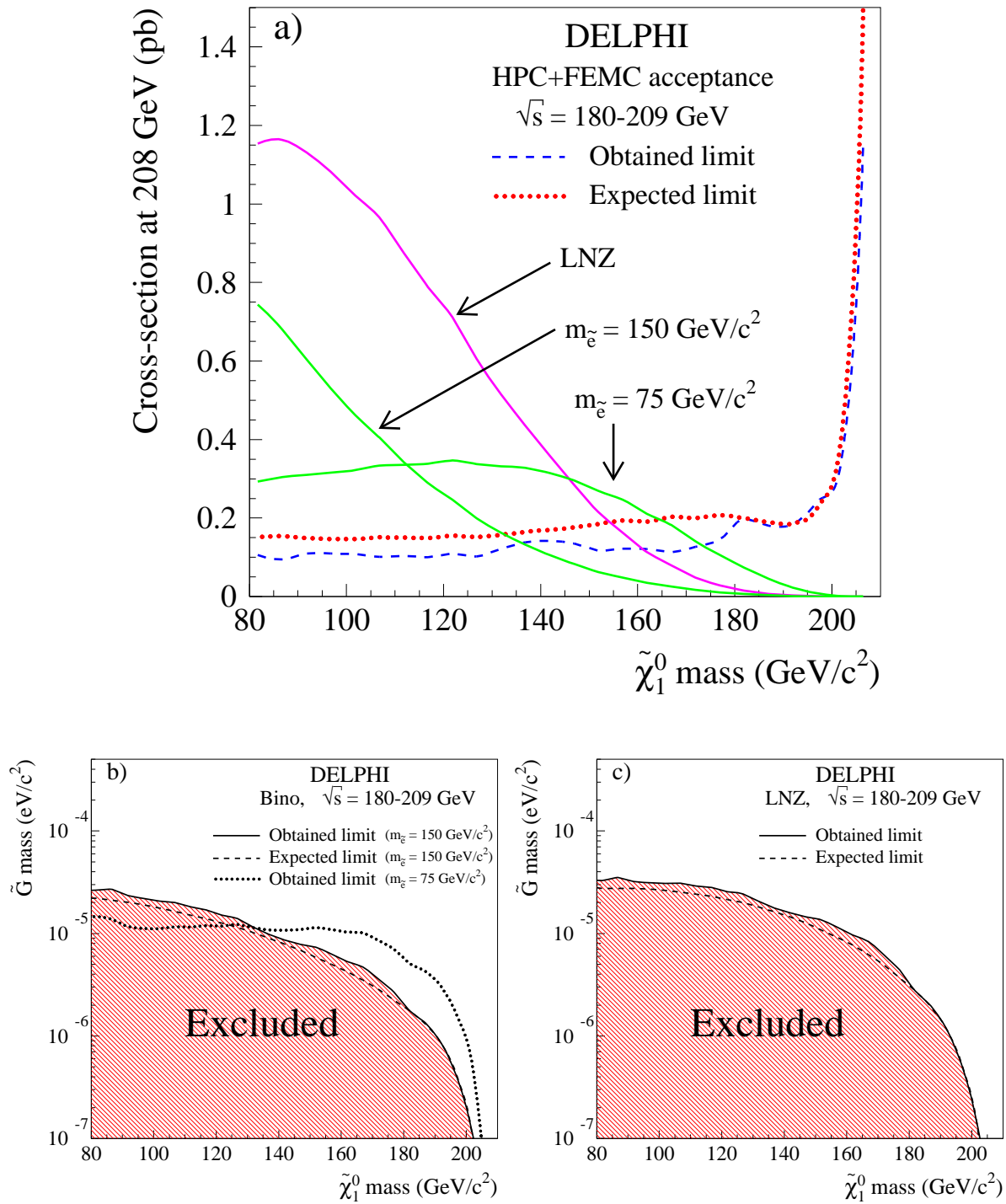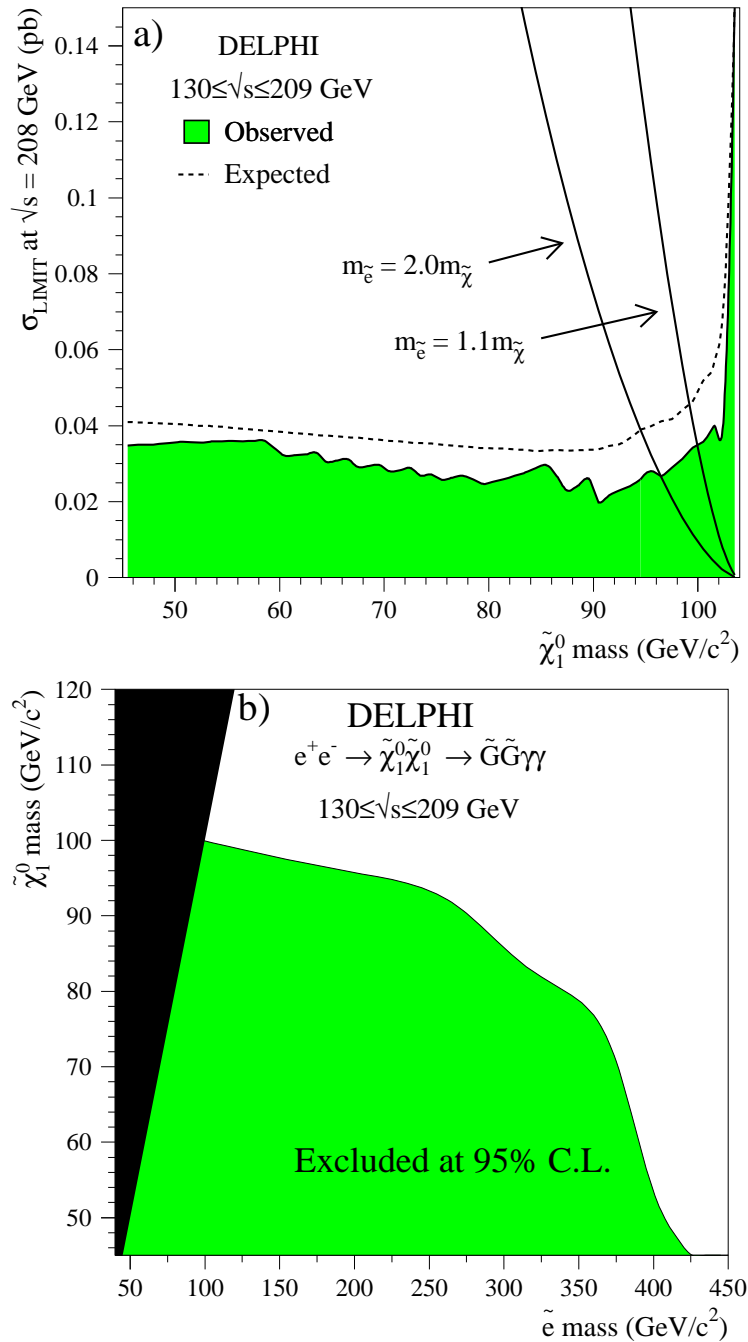
Figure 9: a) Upper limit at 95% C.L. on the cross-section at $\sqrt{s} = 208$ GeV of the process $e^+e^- \rightarrow \tilde{G}\tilde{\chi}_1^0 \rightarrow \tilde{G}\tilde{G}\gamma$ as a function of the $\tilde{\chi}_1^0$ mass. The predicted cross-sections under the assumption that the neutralino is a Bino or as described by the LNZ-model are also shown for $m_{\tilde{G}} = 1 \times 10^{-5}$ eV/c$^2$. b), c) Exclusion plots in the $m_{\tilde{\chi}_1^0}$-$m_{\tilde{G}}$ mass plane.

Figure 10: a) Upper limit at 95% C.L. on the cross-section at $\sqrt{s}$ =208 GeV of the process $e^+e^- \to \tilde{\chi}_1^0\tilde{\chi}_1^0 \to \tilde{G}\gamma\tilde{G}\gamma$ as a function of the $\tilde{\chi}_1^0$ mass and the predicted cross-section for two different assumptions for the selectron mass. The limit was obtained by combining all data taken at $\sqrt{s}$ =130-209 GeV, assuming the signal cross-section scales as $\beta/s$ (where $\beta$ is the neutralino velocity). b) The shaded area shows the exclusion region in the $m_{\tilde{\chi}}$ versus $m_{\tilde{e}_R}$ plane, calculated from the DELPHI data at $\sqrt{s}$ =130-209 GeV.
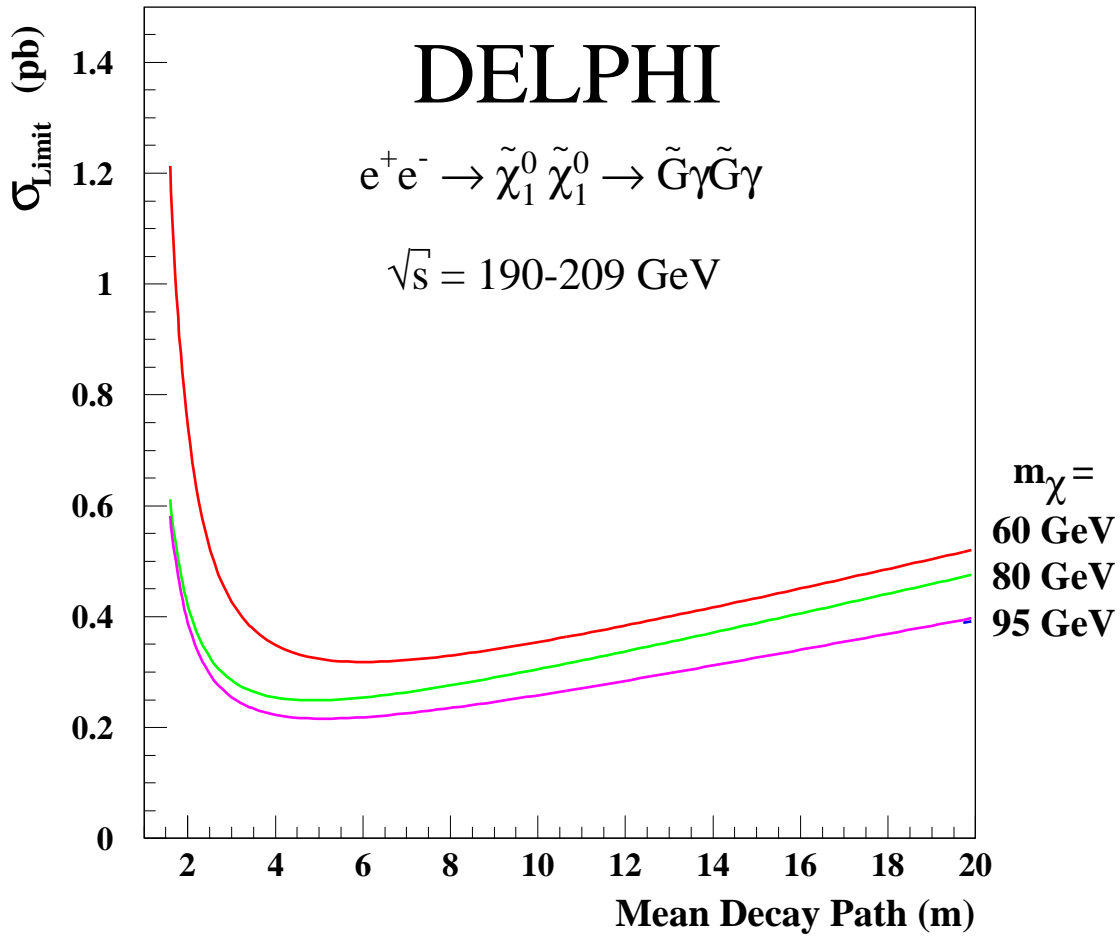
Figure 11: Upper limit at 95% C.L. on the cross-section of the process $e^+e^- \to \tilde{\chi}_1^0\tilde{\chi}_1^0 \to \tilde{G}\gamma\tilde{G}\gamma$ as a function of the $\tilde{\chi}_1^0$ mean decay path for different hypotheses for the neutralino mass. The data collected at $\sqrt{s}$ =190-209 GeV were used for this plot.
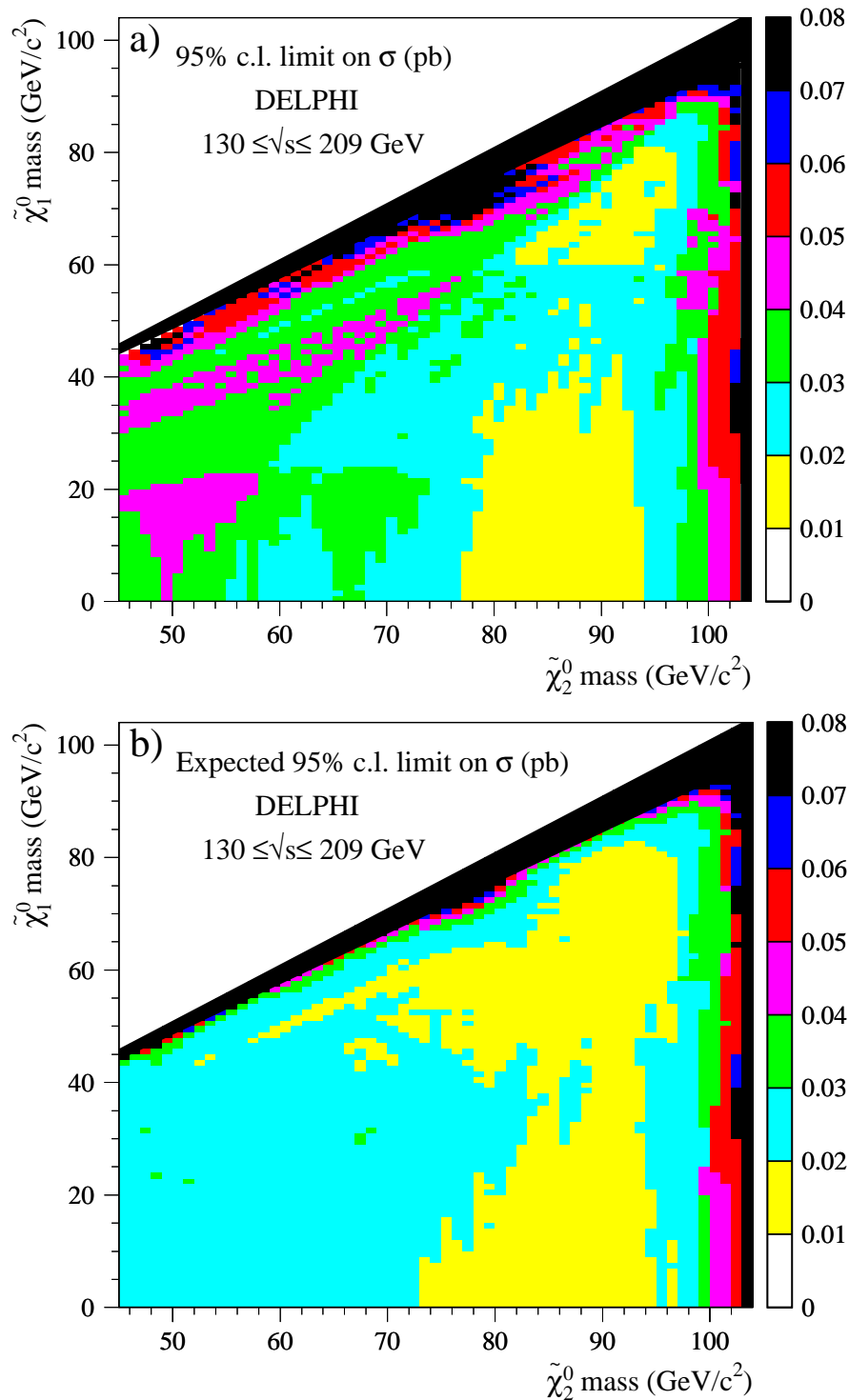
Figure 12: a) The observed upper limit at 95% C.L. on the cross-section at $\sqrt{s}$ =208 GeV of the process $e^+e^- \rightarrow \tilde{\chi}_2^0\tilde{\chi}_2^0 \rightarrow \tilde{\chi}_1^0\gamma\tilde{\chi}_1^0\gamma$ as a function of the $\tilde{\chi}_1^0$ and the $\tilde{\chi}_2^0$ mass. The different shaded areas correspond to limits in pb as indicated by the shading scale on the right hand side. The limit was obtained by combining the data taken at $\sqrt{s}$ =130-209 GeV, assuming the signal cross-section to scale as $\beta/s$. b) The expected upper limit at 95% C.L. on the cross-section at $\sqrt{s}$ =208 GeV of the process $e^+e^- \rightarrow \tilde{\chi}_2^0\tilde{\chi}_2^0 \rightarrow \tilde{\chi}_1^0\gamma\tilde{\chi}_1^0\gamma$.